TÉCNICO LISBOA

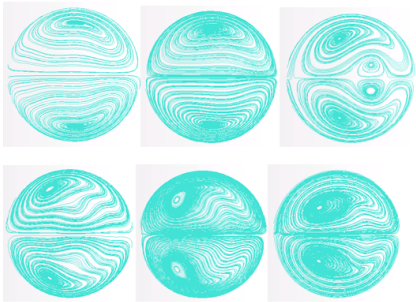

Interaction Fluid Structure on the Laminar Flow in Curved Pipes

Didier Philippe de Andrade

Thesis to obtain the Master of Science Degree in

Aerospace Engineering

Supervisor(s): Professor José Carlos Fernandes Pereira and Professor José Manuel Chaves Ribeiro Pereira

Examination Committee

Chairperson:	Professor Fernando José Parracho Lau
Supervisor:	Professor José Carlos Fernandes Pereira
Member of the Committee:	Professor João Manuel Gonçalves de Sousa Oliveira

June 2014

Dedicated to my Parents.

Acknowledgments

First and Foremost, I would like to acknowledge my supervisor Professor José Carlos Pereira and my co-supervisor Doctor José Chaves Pereira for their advice, support and friendship during this thesis. It has been a privilege to work with them in such a creative and diverse environment.

I am thankful to my colleagues at LASEF, which helped me through technical problems and for accepting me in their group with open arms.

I would like to thank the IST and all the people who work there. For not for them I would not have grown into the person I am today.

Last but not least I would like to thank my family. Where it not for their love and support none of this would have been accomplished.

Resumo

Esta tese centra-se sobre o estudo numérico tri-dimensional da interação fluido-estrutura em tubos curvos semelhantes a uma artéria aorta idealizada. O código de volume finito STAR-CCM+ é usado para resolver o problema de interação fluido-estrutura que é governado pelas equações de Navier Stokes, com o modelo de grandes deslocamentos, num acoplamento iterativo forte. Dois casos são considerados para propósito de validação: tubo à direito colapsado com diferentes espessuras, de modo a validar o modelo de fluido-estrutura e propagação de onda de pressão para a deformação da parede. O estudo principal foca-se sobre a comparação entre o modelo de paredes rígidas e elásticas num tubo curvo sujeito a um escoamento interno pulsado e na artéria aorta. No primeiro caso a simulação é corrida com vários módulos de Young e números de Womersley. Para a circulação sanguínea na artéria aorta idealizada, valores hemodinâmicos são utilizados fazendo-se variar o módulo de Young de modo a observar a influência da elasticidade no escoamento. Os resultados mostram uma validação detalhada do código STAR-CCM+ para o problema da interação fluido-estrutura e resultados fisicamente válidos considerando a influência da elasticidade da parede sobre os vórtices de Dean e sobre o escoamento secundário. A evolução do escoamento com a variação da elasticidade é estabelecida.

Palavras-chave: Artéria Aorta (idealizada), Tubos direitos e curvos elásticos, Interação fluido-estrutura (IFS), Método Volume Finito, Escoamento Secundário, Tensão de corte na parede

Abstract

This thesis is concerned with the numerical study of three-dimensional fluid-structure interaction in curved pipe that resembles an idealized aorta artery. The finite volume code STAR-CCM+ is used to solve the fluid-structure interaction problem governed by the Navier Stokes equations with the large displacement model in a strongly coupled interaction. Two cases are considered for the validation purposes: straight collapsible tube with different thicknesses, for validation of the fluid-structure model and pressure wave propagation for the wall deformation. The main study resides upon the comparison between rigid and elastic walls on the pulsatile flow in a curved pipe and an aorta artery. In the first case simulations are performed for several Young modulus and Womersley numbers. For the blood flow in an idealized aorta artery, hemodynamical values are used whilst varying the Young modulus in order to observe the elasticity influence on the flow. The results show a detailed validation of the STAR-CCM+ code for the fluid-structure interaction model problem and a physical sound result considering the influence of the wall elasticity on the Dean vortices of the secondary flow. The evolution of the flow when varying the elasticity is established.

Keywords: Aorta artery (idealized), Elastic curved and straight tubes, Fluid-structure interaction (FSI), Finite Volume Method, Pulsatile flow, Secondary flow, Wall shear stress

Contents

List of Tables

List of Figures

Nomenclature

Greek symbols

Δt	Time delay of the waveforms.
$\dot{\varepsilon}$	Rate of change of the deformation rate gradient.
$\frac{1}{\tau_M}$	Mass damping coefficient.
μ	Dynamic viscosity.
ν	Kinematic viscosity.
ρ	Density.
σ	Stress vector.
τ	Traction stress.
τ_{ij}	Strain rate tensor.
τ_K	Stiffness damping coefficient.
ε	Strain.

Roman symbols

A	Area.
C_r	Viscous damping matrix.
De	Dean number.
F	Force.
R_c	Radius curvature.
r_i	Internal radius.
Re_D	Reynolds number.
W_o	Womersley number.
x	Deformation.

P	Pressure.
T	Fundamental period of the oscillatory flow.
b	Body forces.
C	Stiffness tensor.
D	Tube Diameter.
E	young Modulus.
h	Thickness.
K	Stiffness matrix.
k	Internal variables.
L, l	Length.
M	Mass matrix.
T	Temperature.
U	Velocity vector.
u, v, w	Velocity Cartesian components.

Subscripts

0	Initial condition.
i, j, k	Computational indexes.
n	Normal component.
x, y, z	Cartesian components.

Superscripts

T	Transpose.

Glossary

CAD Computer-aided design is the use of computer systems to assist in the creation, modification, analysis or optimization of a design.

CFD Computational Fluid Dynamics is a branch of fluid mechanics that uses numerical methods and algorithms to solve problems that involve fluid flows.

MRI magnetic resonance imaging is a medical imaging technique used in radiology to investigate the anatomy and function of the body in both health and disease.

Chapter 1

Introduction

1.1 Motivation

The term fluid-structure interaction (FSI) can be applied to many physical phenomena. A general rule of thumb to classify an application as FSI is if a genuine interaction between a fluid and a solid component occurs. In other words, the properties of the fluid and of the solid must, at the interface level, communicate.

FSI can be divided into two major types of interaction. The most studied one is the thermal interaction aspect. In this thesis we are more interested in the momentum interaction aspect, in which the acting forces influence the movement of the interface and vice versa. The momentum interaction can be even further subdivided into local deformation or a rigid body approach. In pipes, momentum interaction occurs mostly due to pressure forces acting on the solid pipe.

The subject of fluid-structure interaction is immensely vast and can cover almost any field of modern engineering. Some examples of these applications vary from the flutter of a wing, the oscillation of the blades of a compressor or a bridge or even the pulse wave propagation in an artery. This explains why this field has been continuously very active in almost more than a hundred years, and will continue for many more years.

The main factors, which characterize fluid-structure interaction, are: the geometry of the tube, the compressibility of the fluid and the rigidity of the tube. As such it comes with no surprise that one of the most typical practical examples is based upon arterial flow, due to the great value it has for mankind. It is also ideal for an academic study of FSI since all the factors and parameters of interest are found in a single place, which is truly convenient. Since this flow is purely driven by pressure waves, which result from the action of cardiac muscles upon the artery, the pulse propagation phenomena can be studied with ease, in terms of geometry, with computational modelling. Many blood models are available in the literature, from the simplified Newtonian model up to the Carreau-Yasuda model. Differences have been seen in simulations recurring to two and three dimensional models when compared to the *in-vivo* results. It is believed that the main reason for such differences to occur is due to the fact that those models did not take into account wall motion which would somehow make the difference. Despite the

many simplifications, the computational methods used to bridge the ”interaction gap” between the solid and the fluid can be extremely complicated. For example some use the Windkessel model and while others use more sophisticated mathematical and computational models that are specifically designed for a specific case study. This necessity is caused by the particularities of hemodynamic flow, which must take into account the vessel geometry, the ramifications of veins, the behaviour of the wall and the non-Newtonian flow behaviour. As such most numerical results are validated with *in-vivo* experiments.

However most of the research done until now as been mostly based on 1-dimensional (1-D) and 2-dimensional (2-D) models and although the 3-dimensional (3-D) has started to make an appearance, it is still done with for a very specific case with many assumptions and hypothesis. The reason for such occurrence was that, for many years it was believed that the 3-D aspect of both solid and fluid would not have appreciative influence upon the results. Another reason for the lack of 3-D numerical experiments is due to how heavy these computational simulations can be even with the simplest tube. While 1-D simulations would run in a matter of hours, the 3-D model can easily take a couple of days, for example. With the passing of time and the increasingly more resourceful computers available to researchers, some experiments have been made and the issuing results have begun to raise questions upon the previous 2-D assumptions. Also observations on experimental rigs have shown for quite some time that some inconsistencies such as the asymmetric deformations of the solid could not be predicted with the models in use.

Therefore in this thesis the focus point of the simulations that have been run are mostly done with hemodynamics. This was done mainly for the reasons presented above. However it is important to keep in mind that all the results obtained in this thesis can be applied easily to any other field thanks to the adimensional parameters.

Due to the evolution of informatics and physics researchers all around the world have a wider choice of models to use in order to study particular cases. This is true in Medical applications where patient-specific simulations are increasingly being used and are now considered as better representations of clinically relevant models. They are, for instance, utilized to assess the aneurysm risk of rupture, to plan a surgical procedure, to predict the outcome of a treatment, to mention but a few. The reproducibility of patient-specific hemodynamic simulations has been advocated in the literature. Such patient-specific approaches may lead in the future to novel diagnostic and treatment planning tools.

To date, the different approaches to study arterial blood flow include lumped models, 1-D models, 3-D rigid vessels and 3-D FSI (compliant vessels) models. They are all complementary and chosen according to the required level of detail, the extension of the region to consider, etc. For instance, lumped (0-D) or 1-D models are still the models of choice to study pressure and flow wave propagation in extensive regions of the circulatory tree. Even though 1-D models do not allow for detailed flow patterns, they have been shown to produce good quantitative and qualitative predictions of pressure and flow rate waveforms at most of the locations of the arterial tree. They are also easier to couple with other 0-D models, like left ventricle or distal vasculature models.

One-dimensional (1-D) and three-dimensional (3-D) formulations have been used extensively to simulate arterial hemodynamics. Landmark contributions in 1-D modelling include the works of Hughes

and Lubliner [1973], Stergiopulos et al. [1992], Raymond et al. [2010], Olufsen et al. [2000], Formaggia et al. [2003], Sherwin et al. [2003], Bessems et al. [2007], Mynard and Nithiarasu [2008], Alastruey et al. [2011], and Muller and Toro [2013]. Key contributions to 3-D blood flow modelling in deformable vessels include the works of Perktold and Rappitsch [1995], Taylor et al. [1998], Quateroni et al. [2000], Steinman et al. [2003], Cebral et al. [2005], Gerbeau et al. [2005], and Figueroa et al. [2006].

1-D methods have been used to improve our theoretical understanding of hemodynamics, in particular to study the mechanisms underlying pulse wave propagation and also clinically in applications such as wave intensity analysis. Accurate predictions can be made when the flow is predominantly unidirectional and there are no sudden changes in the cross-sectional area.

However, 1-D models require the introduction of additional empirical laws to account for recirculation and pressure losses in the presence of vessel curvatures, stenoses, aneurysms, etc. These geometric complexities are intrinsically captured with 3-D models, which can provide localized hemodynamic quantities such as wall shear stress, particle residence time, etc. Additionally, 3-D modelling enables the use of structurally motivated biaxial constitutive laws and circumferentially varying mechanical properties for the arterial wall and the simulation of complex processes such as the interactions between the arterial wall and medical devices. Nevertheless, 1-D models typically contain far fewer DOFs in comparison with 3-D models (on the order of 10E3 vs 10E6), and the simulations can be executed in a matter of minutes on a personal laptop computer.

In contrast to 1-D models where gross features of flow (i.e., pressure and flow) are studied, 3-D rigid wall models are used to obtain details of the flow patterns in specific arterial locations of particular physiological or pathological interest, such as at bifurcations, at the aortic arch, abdominal aorta or cerebral aneurysms. In the majority of 3-D studies the fluid flow is determined by assuming wall is rigid and that any motion does not affect the flow. This assumption simplifies the numerical approach and is fully justifiable only in the cases where the wall motion is relatively small. However, when important arterial wall deformations are encountered during the heart cycle, such as in the order of 10-15$\%$ for the aorta, it becomes essential to include this effect also. a fluid-structure interaction (FSI) approach is necessary to address this issue. FSI modelling for a patient-specific vasculature is still a very complex task to handle and is computationally expensive.

1.2 Numerical Methods for fluid structure interaction

The study of FSI in computational models has evolved considerably with the passing decades. From 1-D solutions to 3-D numerical schemes coupled with advanced physical models, there is a wide range of work done on the subject. Thanks to the progress made in modelling fluid flow and the solid structure behaviour of materials, the interface question is starting to attract interest from the scientific community. The communication of information through boundary conditions can be categorized into four options based on the type of coupling between fluid and solid:

The first method that was used is the *non-iterative over all time* approach. It is most commonly known under the term *uncoupled approach*. As the name suggests the fluid and solid equations are

solved separately in the whole time domain. Beginning with the fluid in order to obtain the velocity and pressure fields, the pressure at the interface obtained is then specified as a time-varying boundary condition for the solution of the solid equations.

The second method is *iterative over all the time*. It shares many similarities with the *non-iterative* approach, however the solution for the solid, displacements or velocities, is used as time-varying condition on the fluid. Then the process is repeated by solving the fluid, passing the pressure boundary condition to the solid, solving then the solid etc. The process is then repeated until convergence of the solutions is achieved.

The third method can be described as *non-iterative over each time step*. Here the boundary conditions are passed between fluid and solid at the end of individual time steps, however no iterations from fluid to solid solutions take place in the time step. In some cases time step may not be the same for the components. This can be referred to as non-iterative over unequal time steps.

The fourth method is *iterative over each time step*. Here the fluid equations are solved in a single time step and the pressure solution is applied as the boundary condition for the solid equations. Afterwards the solid equations are solved in a time step and the resulting pressure becomes the new boundary condition for the fluid. The process is thus repeated, in the same time step, until convergence is reached. Then another time step begins and the process is repeated.

When using *non-iterative over all time*, *non-iterative over time step* and *non-iterative over unequal time steps*, one should be aware that since the fluid solution is computed before the solid one, the coupling is only one way. This goes against the concept of FSI introduced before and thus these methods should be avoided. For better results the use of multiple iterations is recommended to ease convergence and achieve a more realistic result (mostly in the first couple of time steps).

Two problems arise from the discretisation process, the treatment in time and space. Since the numerical method itself is not the object of this thesis, only a brief overview will be presented. For the time treatment of the fluid and solid, and using the conventional terminology in literature, the numerical methods are divided into partitioned methods and monolithic methods.

The first one partitions the fluid and the solid solution, meaning that the fluid and solid equations are solved alternately and the enforcement of kinematic and dynamic interface conditions is asynchronous. Usually this results in the use of two separate software codes which is usually avoided due to the size and complexity of the simulation. Another drawback of this approach is the computational hardware requirements in order to run such codes.

The second method comprises two separate sets of equations for fluid and solid and coupling the fluid dynamics and structural dynamics implicitly and solve them synchronously at their coincident interface. The discretised equations are solved by sub-iteration until convergence or a stopping criteria is reached in a time step. The main benefit of this method is it's stability and energy conservation. However the method is still rather quite complex and computational demanding because of the sub-iteration.

The beginning of fluid structure interaction can be traced from the 19th century, with the basic equations and theories being written then. However it is only in the 1970s that computational FSI truly begins.

The first studies on wave propagation, using incompressible fluids in elastic tubes, for instance rubber

hose and blood vessels were published in Young [1808] and for compressible fluids by Korteweg [1878].

Reuderink et al. [1989] presented one of the first studies of pulsatile flow in elastic arteries with one dimensional wave propagation. Using both linear and non-linear theory in blood vessels and comparison with experimental data brought forth the conclusion that linear model seemed more appropriate. the linear model can compute better the damping of the wave. However the non-linear terms in mass and momentum conservation equation showed to be significant.

Perktold and Rappitsch [1995] used an iterative approach for the same flow field examined by Reuderink et al. [1989]. The boundary conditions of the flow problem, the inlet and the outlet pressure, were obtained from experimental data. The results were compared with models of rigid and distensible walls and the last one provided more realistic results.

Steinman and Ethier [1994] used a similar method to Perktold and Rappitsch [1995]. An analytical approach was used to study the effect of wall distensibility of a flow on end-to-side anastomosis. The outlet pressure was obtained using wave theory. They concluded that when comparing the rigid-wall simulations, the wall shear stress showed moderate changes. This, according to them, is due to models that neglect the wall distensibility that cannot predict accurately the behaviour of local pressure gradient fields, as well as velocity profiles.

Henry and Collins [1993] focused on the prediction of wall movement in elastic tubes using an iterative approach as a coupling method. The inlet and the outlet pressures were fixed to a certain value. Validation of the model used was made with analytical solutions.

Taylor et al. [1998] used a numerical method to model only the fluid of a pulsating flow in straight arteries. For boundary conditions of the fluid-solid interface, they used zero wall motion. Womersley [1957] analytical solution was used for validation. Their main concerns was that the methods for FSI available at the time would produced enormous amount of data and took a considerable amount of computational time.

Bathe and Kamm [1999] used the iterative over time step coupling approach in modelling pulsatile flow in stenotic arteries. The boundary conditions at the inlet and outlet came from experimental data. Validation with experimental data was made and the model was also compared with other mathematical models. By comparing arteries with different degrees of stenoses, they found that inviscid predictions were lower, as expected, than the computed pressure drops due to the fact that the viscous losses were neglected. Their main conclusion was that the bulk of the pressure drop into the stenosis is due to the convective acceleration of the flow.

Konig et al. [1999] modelled only the fluid using a moving boundary. Inlet and outlet pressures were fixed using reference values. Validation was made with experimental data. High and low viscosity models were compared and better results were obtained with the high viscosity model.

Tang et al. [1999] studied stenotic arteries using both thick and thin wall models. They observed that the stenotic severity and asymmetry in thick wall models changed not only the wall geometry, but also the stiffness of the tube wall and this affected the wall deformation. The maximum shear stress from the thick wall asymmetric stenotic tube was considerably lower than that from thin wall model due to increased stiffness of asymmetric stenosis. They concluded that arteries have a complex structure and

should not be treated as a homogeneous material.

Zhao et al. [1998] and Xu et al. [1999] used thin and thick wall models and the thick wall model provided more realistic results. Data from Magnetic Resonance Imaging (MRI) of real patients was used to compare with the computational model. They encountered a significant problem when comparing results due to large anatomy variations. Neither the compliant behaviour of the vessel wall or the non-Newtonian behaviour of the blood was taken into account, since the authors considered these not to be essential.

Jensen and Heil [2003] investigated self-excited oscillations in 2-D collapsible-channel flow. They divided a tube of arbitrary length into three sections, the entry and end section are constrained while the middle is subjected to transmural pressure, in order to assess the influence of the flexible tube length in oscillations. Low Reynolds flow was used in the simulation. Validation was made through comparison with previous work. They deduced a critical Reynolds number for self sustained oscillations. However the absence of dependence of the length in the equation was considered to weaken the result and showed the need to improve the expression.

Blackburn and Sherwin [2004] experimented with axisymmetric constricted tubes in order to simulate stenosed arteries. They observed three-dimensional instabilities and transition to turbulence of steady flow, steady flow with an oscillatory component and an idealized vascular pulsatile flow. Transition was found to be localized with relaminarization occurring further downstream.

Marzo et al. [2005] studied three-dimensional collapse of steady flow in finite length tubes with varying thickness. Validation was achieved by comparing the resulting data with experimental pressure-area relationships for thick-walled tubes. They discovered that the Young wavespeed could be lower between buckling and osculation for thick tubes than thinner ones.

Luo et al. [2008], interested in the instabilities present in collapsible channel flows, made extensive mapping of the unsteady behaviour and linear stability of the flow in a collapsible channel using a fluid-beam model. The Reynolds number used was in the range of 200 to 600. The main factor for the appearance of instabilities was the reduction of wall stiffness (or effective tension). One of their discoveries was if the instabilities were small enough, various modes of collapse could be observed. Another conclusion from the simulation showed that the self-excited oscillations were dominated by modes 2-4 near their corresponding neutral curves. Validation was achieved with comparison of existing analytical models.

The present work is focused on Finite Volume method, 3D and unsteady flow with fluid-structure interaction between the blood flow and the arterial elastic vessel. Consequently a literature review was undertaken and sub-divided into the major topics related with the present configuration:

- Wave propagation in straight tubes.

- Collapsible tubes.

- Pulsatile flow in a curved pipe.

- tapered tubes.

The following sections summarises reviews on these topics.

1.3 Literature Review

1.3.1 Wave propagation in straight tubes

This section focus is on the literature review on wave propagation in straight tubes. In the first part the theoretical models are reviewed, followed by the review of experimental models.

The first researcher to study the transient motion of fluids in pipes, elastic tubes, convial vessels and blood circulation was Young [1808]. A formula was proposed by him for the velocity of pressure waves in an elastic tube with thin, homogeneous and isotropic wall, filled with an incompressible fluid.

Witzig [1914] also investigated the wave propagation by modelling thin-walled flexible tube by solving two dimensional linearised Navier-Stokes equations. He showed that the effects of viscosity of the fluid are present in fluid velocity profiles.

Womersley [1957] is perhaps the most famous in the literature. His results were compared countless times against other theoretical models and was improved. He solved the two-dimensional linearised Navier-Stokes equations for thin-walled isotropic infinitely long elastic tubes filled with viscous Newtonian fluid. Both unrestrained tubes and tubes constrained in the axial direction were used.

Atabek [1968] studied analytically the unsteady flow near the entry of a circular tube and showed that the entry length varied with the time through the cycle, as do the boundary layers which determinate it. Atabek and Lew [1966] extended the Womersley theory to initially stressed thin walled tubes in the axial and circumferential direction. They discovered the existence of two waves: radial and longitudinal that can be predicted with the Womersley theory even if he did not found out himself. With the continuity and momentum equation the frequency equation can be obtained. The two roots of this equation gives the velocity of the propagation of the two waves.

Mirsky [1968] combining the Womersley models with longitudinal tethering and extended it to include tubes with orthotropic walls. Cox [1969] using the work previously done, organised it in three categories: thin-wall with no constraint; thin-wall with longitudinal constraint and thick walled tubes. At the end of his research he presented a table with the models developed previously.

Atabek [1968] continued his previous work, this time using the membrane theory of shells on orthotropic tubes. He concluded that the propagation properties of the slower waves are very slightly affected by the degree of anisotropy of the wall. In the case of faster waves the velocity of propagation decreases as the ratio of the longitudinal modulus of elasticity to circumferential modulus decreases. If tethering is used the faster waves are completely attenuated, while the slower ones do not suffer any alteration. These findings were in agreement with the Womersley theory and Mirsky [1968] s' work. He made the remark that for the theory to be complete and thus provide a realistic result for use in arterial

systems it would need to include taper, branching and the viscoelastic properties of the wall.

Ling and Atabek [1972] first introduced the non-linear terms of the Navier-Stokes equations as well as the non-linear behaviour and large deformations of the arterial wall. Experiments were also performed. The conclusions reached at the time showed that their non-linear theory predicted the velocity profiles with better precision than the linear one. The wave of the wall shear predicted by the linear theory is very close to the one predicted by the non-linear theory.

1.3.1.1 Experimental models on straight tubes

von Kries [1883] was among the first to take an interest in measuring the pressure pulse in human bodies. In order to validate his theory he performed experiments on rubber hoses. The experiment itself was made from thin-walled rubber hose with 4 to 5 m long and 5 mm diameter which was attached to a constant head reservoir.

Klip [1962] realised that propagation velocity and damping of pressure waves in arterial systems could be used for diagnostic purposes, as such he performed a series of experiments on tethered tubes of great length. In his experiment he used 60 m long tube, considered as being homogeneous, isotropic and viscoelastic. A piston was used to propagate a pressure wave. The tube is straight for 4 m and afterwards wounds up in spiral. He detected no reflections in his experiment. Various water-glycerine based solutions were used. The measuring apparatus consisted on a manometer for the pressure and an electric phase meter for the phase differences. He took into account both thick wall and thin wall tubes. Comparing his results with other methods of calculation for the phase velocity and he found that they were in good agreement with Womersley's results as well as with Moes-Korterweg predictions. Damping, however, showed some differences.

Ling and Atabek [1972] simulated blood flow in dogs. A composite straight structure of silicon rubber and corrugated nylon fibres was used. The diameter of the tube was chosen as to be representative of a medium sized dog and the thickness was around 1 mm. The fluid used was a glycerine-water solution. The pressure and pressure gradient were measured with an interval of 50 mm of distance using pressure transducers, while the velocity profile was measured with a hot-film probe. Wall shear stress was also measured. The variation of pressure-radius was photographed.

Nerem et al. [1971] investigated the transition to turbulence in the aorta and related these results to equivalent steady flow ones in which the similarity parameters were the wave number and the Reynolds number.

Liepsch and Moravec [1984] made a replica of the femoral artery using rubber and performed experiments of pulsatile flow. Later Deters [1986] made a silicon rubber cast from luminal mould of an aortic bifurcation where they measured phase fluid velocity using LDV on a single point of the wall. By integrating the velocity they managed to obtain the motion of the wall while the shear rate at the wall obtained dividing the fluid velocity by the distance from the velocity measuring point to the wall.

Until 1986 the Womersley theory had been only tested for tethered tubes. Gerrard [1985] wanted to determine the behaviour of infinitely long tubes. For his experiment he used isotropic latex rubber tubes, with small viscoelasticity. He put together two tubes, of 15 m length inner diameter 6.2 mm and

1.8 mm of thickness, with glue. The pressure wave was formed with the help of a piston. The fluid used in the experiment was water. In order to allow free motion the tube was suspended from the ceiling using cotton sewing threads 100 mm apart. The tube is considered as behaving as a semi-infinite tube over almost all its length. No reflections were detected. When comparing the experimental results with the predictions from using the Womersley theory, it was found that apart from the entrance length the data was in good agreement. This was assumed as being the effect of having a closed end far from the piston, which reduced the amplitude obtained with the infinite-tube theory. Gerrard [1985] made experiments with tethered tubes with 30 m long and the ensuing results were in good agreement with those obtained by Klip [1962].

van Steenhoven and van Dongen [1986] wanted to study the aortic valve closure apart from the pressure wave phenomena. Their experiments consisted on water filled latex tube 0.6 m long with 18 mm inner-diameter and 0.2 mm of thickness. In this experiment transmural pressure was applied at one end of the tube. Pressure was measured with two catheter-tip manometers, while the wall deflection was measured with a photonic sensor and the flow volume was measured electromagnetically. Their measurements of the wall displacement were in good agreement with the ones obtained by Gerrard [1985]. With the experimental results they were able to determine the viscoelastic properties of the tube. They also compared the resulting data with the one dimensional non-linear theory for the wall shear stress, which was solved numerically using the method of characteristics. The wall of the tube was assumed as being viscoelastic and wave reflections were taken into account. One of the conclusions that resulted from their experiment was that the wall viscosity is a dominant factor in the gradual flattening of the waveform. Another conclusion was that the local change in compliance generated wave reflections, which was expected, and it had also a strong influence on the rise-time of the wave front. The major conclusion, however, is that the pressure jump of the wave-front decays while propagating upstream.

Horsten et al. [1989] used the same experimental set up as van Steenhoven and van Dongen [1986] with the difference of using 0.9 m long tubes to simulate wave propagation. One dimensional linear theory was used to compare the resulting experimental data and they found that good agreement was achieved for small pulsed shape waves. Several linear models were compared with the wall behaviour that was obtained and there was no major differences amongst them. It was found that the one dimensional Womersley linear theory, in which the fluid is treated as being incompressible, managed to describe with reasonable accuracy the propagation phenomena. On the other hand the wave velocity was found to be underestimated and the damping was overestimated. The non-linearities are thought to be partially responsible for this discrepancy. Another one of the possible causes could be the rigid support.

Reuderink et al. [1989] compared the one dimensional linear and the non-linear theory describing the pulse wave propagation in a uniform viscoelastic tube. The experiment consisted in a 1 m long latex rubber filled with a salt solution and a pneumatically driven piston to initiate the pulse wave. The pressure was measured at different positions of the tube using a manometer. An attempt was made to measure pulsatile diameter changes with an ultrasonic transit-time technique but, according to them, the influence on the wall motion was present and thus the results were inconclusive. Their experimental data

showed that the pressure vs cross-sectional area relation was non-linear for the pressure changes. After comparing results with the linear and the non-linear models, they concluded that despite the non-linearity of the system, the linear viscoelstic Womersley model can describe the pulse wave propagation with good accuracy. Neglected frictional losses due to wall viscosity and fluid viscosity being underestimated was found to be the reason to the discrepancies that arose from the experimental data and the non-linear model. As such, non-linear models predicts small damping and formation of shock waves, which are not observed experimentally.

1.3.2 Collapsible tubes

Fluid flow in elastic tubes is a large displacement fluid-structure interaction problem encountered in biofluid mechanics (Meng et al. [2005]), peristaltic pumping (Shapiro et al. [1969]) and other applications. The flow in a compliant channel is related to many physiological applications. For example, blood flow in arteries and veins, urine flow in the urethras and air flow in the lungs. The compliance of the wall has a great influence on the transport of fluid, and thus will elicit important biological effects on the living body. Human snoring and wheezing are two of the phenomena related to the oscillation of walls in human airways.

Motivated by the fundamentals of physiology, this area has attracted many researchers during the past 30 years. Experimental studies date back to the 1960s and 1970s. Large amount of literature references were found from the 1980s and 1990s.

Several works on the study of flows in collapsible tubes and channels have been well documented based on the intended biological applications (Grotberg and Jensen [2004]; Kamm and Pedley [1989]; Pedley [1980]; Shapiro [1977]). Biofluid mechanics is important to the flow of fluids through vessels in the human body, as numerous fluid conveying vessels are elastic and subject to buckle non-axisymetrically when the transmural pressure falls below a critical value (Heil [1997]). The interactions between the internal flow and wall deformation of these flexible vessels determine the biological function or dysfunction. The examples of such vessels are the veins above the level of the heart, the airways during forced expiration the pulmonary capillaries and the blood vessels in the heart muscle during systole (Conrad [1969]; Pedley [1980]). Holt [1941] investigated how the collapse of veins might affect peripheral venous pressure. He set up a model where water flowed through a more rigid pipe. The exact flow and wave propagation in distended tubes was well understood, whereas the flow structure in collapsed vessels has been less investigated.

The problem of flow in collapsible tubes was extensively studied experimentally by many authors e.g. Conrad [1969]. The Starling Resistor is a classical bench-top experimental set up which was widely used to investigate flow through elastic tubes relevant to many applications. This involves a pressure chamber that encloses a finite-length elastic tube mounted between two rigid tubes and a fluid is pumped through the tube at a steady volume flow rate. In the standard experiment the pressure could be independently controlled. The behaviour of the system is studied by adjusting the controlling parameters such as the ambient pressure both in the chamber and at the outlet, the material property of the compliant tube as

the tension and the flow rate. A steady flow was obtained in certain range of controlling parameters. Beyond this range, however, complicated phenomena such as flow-induced oscillations occurs.

The tube's large deformation during the buckling was found to lead to a strong interaction between the fluid and solid mechanics which was described by non-linear shell theory (Heil [1997]). Steady flow through a collapsible tube was found to be a multiple-valued function of the pressure drop across it, named as flow-controlled non-linear resistance, QNLR (Conrad [1969]), where a systemic experimental pressure flow curve for both steady and unsteady flow conditions were presented. The significant system parameter for changes in tube cross-section was transmural pressure, which in turn affected the flow geometry. The typical fluid-structure interaction problem involving the flow passing a collapsible tube was studied both experimentally and theoretically, and represented with a relationship between transmural pressure and cross-sectional area and the factors area which influenced it.

On the other hand, Lyon et al. [1980] proposed the hypothesis for the pressure-flow relationships by the waterfall model studied in a Starling Resistor, described only for flows with lower Reynolds numbers. The minimum Reynolds number for self excited oscillations was precisely determined experimentally by Bertram and Tscherry [2006]. There are few theoretical investigations of both the flow and the wall mechanics in three dimensional collapsible tubes. In addition, the wall deformation and fluid flow was modelled using geometrically nonlinear shell theory and lubrication theory respectively. If the transmural pressure acting on the tube is sufficiently negative then the tube buckles non-axisymmetrically and the subsequent large deformations lead to a strong interaction between the fluid and solid mechanics (Hazel and Heil [2003]).

The extensive experimental and theoretical contributions made by several authors mentioned above are of great value for the scientific community as well in the many biomedical and biomechanical applications. These enable the better understanding of the laminar and turbulent flows of Newtonian fluids though collapsible tubes and the solid mechanics of the tube. In contrast, there is little literature on the experimental flow characteristics of non-Newtonian fluids through elastic tubes under the influence of different transmural pressures involving the interaction of the deformed tube wall with the fluids. In addition, there is also little information available on the unsteady-periodic flow or peristaltic-squeezing of elastic tubes for transport of such fluids.

The investigation methods for the shape of the deformed elastic tube and the corresponding flow fields are also not yet well established. The local tube cross sectional area was measured by an electrical impedance technique or ultrasound imaging or remote sensing technique. The cross section was assumed to remain the same throughout the tube as the same amount of liquid was flowing with the same mean velocity through each cross section at any given time. In contrast, different cross-section of vessel or rubber tube showing changes in shape during oscillations of pressure was also observed. Kresch and Noordergraaf [1972] proposed a mathematical analysis for the cross-sectional shape of a flexible tube as its internal pressure varies. Quantitative results were presented in terms of the physical parameters of the tube, such as wall thickness and Young's modulus.

The early theoretical studies were based on ad hoc one-dimensional models. These works did explain some phenomena observed in experiments. In order to perform more realistic simulations,

Pedley [1992] first studied a steady two-dimensional flow with collapsible wall at low Reynolds number using Stokes approximation for the fluid. Later, two-dimensional simulation by solving full Navier-Stokes equations was done by Luo et al. [2008] for steady and unsteady flows. The wall was modelled as an elastic membrane of zero thickness. In this model, the wall only moves vertically, the longitudinal stretch and bending stiffness of the material are neglected. Heil [1997] performed a three-dimensional simulation of flow through a collapsible tube using Stokes approximation for the fluid and a shell model for the wall. Recently, a more realistic model was proposed by Cai and Luo [2003], in which a plane strained elastic beam with large deflection and incrementally linear extension was used to replace the membrane. Bathe and Kamm [1999] solved the two-dimensional Navier-Stokes equation for the fluid and two-dimensional equilibrium equation for the solid elastic wall. In these simulations mentioned above, the effect of certain control parameters on the fluid-solid system was studied by carrying out "numerical experiments".

In almost all these numerical studies, finite element method (FEM) was chosen as their numerical scheme, Takemitsu and Matunobu [1988] was the only exception in which finite difference method (FDM) was used. X.Zhang et al. [2005] presented an alternative approach to tackle this problem: finite volume method (FVM) is used to solve the fluid equation and finite difference method (FDM) is used to solve the membrane equation. Although FVM is the most popular numerical method in the area of computational method fluid dynamics (CFD), in research areas where the fluid and structure interaction (FSI) is involved, FEM still dominates. This is because FEM is traditionally the only choice for structural analysis. It is only recently that FVM has begun to play a role in this area. The advantage of FVM lies in its simplicity of formulation and attractive local conservative properties.

Many physiological conduits transport viscous fluids within our body. Because of their high flexibility, these conduits may collapse non-axisymmetrically under particular conditions of external and internal fluid pressure. When this phenomenon occurs, the buckled vessels become very flexible and small changes in transmural pressure P_{tm} (internal minus external pressure) may induce large displacements. This strong interaction between fluid and structure gives rise to a number of interesting phenomena, including flow-rate limitations, pressure-drop limitation and a tendency to self-excited oscillation.

In the cardiovascular system, veins above the level of the heart and outside the skull collapse due to hydrostatic reduction of blood pressure. This assumes particular importance in subjects with long necks, especially giraffes. Flow-induced collapse of cardiovascular vessels is believed to play an important role in the supply of blood to many internal organs. Moreover, dynamic flow-induced collapse of blood vessels downstream of atherosclerotic stenoses may cause plaque rupture, which can lead to the occlusion of the vessel lumen distally, with potentially lethal consequences in the case of the carotid artery. In the large airways, flow-induced oscillations are believed to give rise to a number of different role in speech production. During micturition, the urethra behaves like a collapsible tube, and accordingly can exhibit flow-limitation effects.

Given its importance and complexity, the topic of flow through collapsible tubes has been studied for over 30 years. However, the full understanding of this physical phenomenon still represents an unsolved challenge. Kamm and Pedley [1989] reviewed the subject briefly; a more comprehensive review of the

biological examples and the theoretical and computational developments is given by Heil and Jensen [2003], while Bertram [2003] has reviewed the experimental side of the subject, and applications in medicine and technology. Experimental investigations on a Starling resistor prototype of the system have revealed a rich dynamic behaviour, with various types of self-excited oscillations. To reveal the mechanisms of such oscillations, much work has been carried out, but most is limited to 1-D or 2-D models.

One-dimensional models adopt a large number of ad hoc assumptions that limit any systematic improvement. Two-dimensional models of a collapsible channel are based on a more rational approach, and in principle could be realized in a laboratory. However, only a 3-D study can provide the full picture of a collapsible tube, which exhibits strongly 3-D behaviour. Owing to the extensive computational resources required and the high non-linearity of the system, to date there is only limited published work on 3-D thin walled tubes. Hazel and Heil [2003] investigated the steady flow through thin-walled elastic tubes for a finite Reynolds number. In their finite-element approach, they solved the steady 3-D Navier-Stokes equations simultaneously with the equations of geometrical non-linear, Kirchhoff-Love thin-shell theory. One of the assumptions underlying thin-shell theory is that the wall thickness of the tube is some 20 or more times smaller than its radius. Considering that much experimental work is on thick-walled tubes, it is important that 3-D numerical simulations are not restricted to thin-shell theory.

1.3.3 Pulsatile flow in curved pipe

The terms unsteady, pulsatile or oscillatory are commonly used in the literature to describe flows in which velocity or pressure depends on time. Oscillatory flow is a periodic flow that oscillates around a zero value. Pulsatile flow is a periodic flow that oscillates around a mean value not equal to zero: it is a steady flow on which is superposed an oscillatory flow.

Study of periodic flows trully started in 1950. The first investigations of oscillatory and pulsatile flows in straight tubes dealt with the mathematical aspects of the fluid motion. These first analytical studies for a fully developed regime made it possible to determine the characteristic parameters controlling the flow.

In oscillating flows in tubes, the interaction between viscous and inertial effects produces a velocity profile with significant deviation from the parabolic shape of steady flow.

Takayoshi and Katsumi [1980], in an analytical study of a fully developed pulsated flow in a circular tube, showed that when the oscillation motion is slow, the flow has a parabolic velocity distribution with deceleration in the tube centre during the deceleration phase. When the oscillation frequency is kept weak, a return motion is observed in the flow centre; when the oscillating component of the pulsated flow becomes stronger, viscosity effects are confined near the wall for large-amplitude velocity ratios and the return motion observed in the tube centre for the slow oscillations is pushed towards the wall. This return flow develops when the balance of the flows constituting the pulsated flow favours the oscillating component.

Ohmi et al. [1981] classified the different regimes in pulsatile flow using the influence of the non-

dimensional frequency parameter. In the quasi-steady region, the flow conforms to steady flow. The intermediate region is identified as the passage from the steady to pulsatile flow, with observable influences of flow oscillation, and the inertia-dominant region occurs when the inertia effect itself dominates the flow.

In steady laminar flow through ducts, the effect of even very slight curvature is not negligible. The presence of curvature in ducts generates a centrifugal force. In steady flow, this centrifugal force induces a pressure gradient in the fluid and a secondary flow, a pair of counter-rotating symmetrical vortices called Dean cells, in the duct cross-section. Steady fully developed laminar Newtonian curved flows of circular cross-section have been studied extensively; some of the previous work is presented in Berger et al. [1983a]. The first solution to the flow in curved tubes was suggested by Dean, who solved the axisymmetric laminar flow problem and demonstrated the existence of secondary flow.

Dean flow is thus the flow of fluid in a curved duct, and the corresponding control parameter is the Dean number. Beyond a critical value of Dean number appears another pair of counter-rotating vortices, called hereafter Dean vortices, on the outer (concave) wall of the duct. These vortices are due to Dean instability, one of the large family of centrifugal instabilities to which the Taylor-Couette and Gortler instabilities also belong.

Lyne [1971a] was the first to highlight the complexity of the fully developed laminar oscillatory flow in curved pipes. He carried out a Dean analysis by introducing a flow generated by a pressure gradient varying sinusoidally around zero and demonstrated the appearance of a new vortex pair over and above those observed in the steady case. The appearance of the Lyne vortices results from an increase in the frequency parameter in a pulsating curved duct flow. The frequency parameter in pulsating curved duct flow. The frequency parameter (Womersley number) can be defined as the ratio between the inertial forces due to the local acceleration and the viscous forces determining the movement over a time scale equal to the oscillation period. This parameter affects the relative size of the boundary layer disturbed by the pulsation compared to the size of the boundary layer in steady flow. A low frequency parameter implies a large viscous layer near the wall, or a large oscillation period compared to the viscous diffusion time. In this case the secondary flow field is similar to that obtained in a curved pipe in stationary flow over the whole pulsation cycle. When the frequency parameter increases, the viscosity effect is reduced to the wall and the inertial effect increases in the central area of the section. The imbalance between the forces favours the centrifugal force in the cross-section centre; near the external wall, the tangential velocity becomes larger than the radial velocity, so that fluid particles initially close to the flow centre migrate towards the external wall. The vortices thus formed are stretched, and their respective centres move slightly to the top and bottom of the section in a symmetrical way. The axial velocity has an annular form that presents a peak near the wall, corresponding to the velocity at the vortex centres, and a valley in the cross-section centre. The valley arises because, in the central area, the fluid no longer obeys the axial pressure gradient variation, compared to fluid close to the external wall.

When the frequency parameter increases significantly, the fluid close to the concave wall stops the secondary flow and a stagnation zone appears close to the concave wall. The pressure gradient becomes thus higher than the centrifugal force in the section centre and at certain times, the fluid in the

stagnation zone and close to the concave wall begins a rotational movement. Close to the external wall an additional pair of vortices appears that develops and occupies the section centre while pushing the centre of the previous vortices to the top and bottom of the pipe cross-section. This secondary flow, consisting in four vortices, all counter-rotating is the Lyne instability. The formation process of the Lyne secondary flow is much more complicated than previously thought, since it causes an alteration in the force balance (centrifugal force, pressure gradient, and inertial force). The various stages of this process can nevertheless be shown schematically.

The frequency parameter is not the only factor that influences the appearance and evolution of the Lyne vortices: the flow Reynolds number has also an important effect here. For relatively low Reynolds numbers, the secondary flow consists of two Dean cells, with low intensity compared with the cases of large Reynolds numbers. For large Reynolds numbers, the profile of the main velocity radial distribution presents a maximum near the concave wall. Hamakiotes and Berger [1988a] showed that, for a particular configuration, when low stationary Reynolds numbers are used (below 400), the secondary flow is similar to that without oscillation at any time in the period.On the other hand, the cells observed for large Reynolds numbers (above 600) follow the Lyne deformation, during the acceleration phase.

Lyne vortices are also sensitive to the velocity amplitude ratio defined by the fraction of the maximum speed of the oscillating component and the mean speed of the steady regime. A small value of this parameter induced a quasi-stationary flow (Toshihiro et al. [1984]). Indeed, a low value causes the dominance of the stationary component on the oscillating component. The secondary flow under these conditions is similar to Dean flow over the whole pulsation cycle. The velocity field distributions are not dependent on the frequency parameter. On the contrary, when the velocity amplitude ratio increases the velocity distributions become complicated and an annular flow appears. The secondary flow shows a particular field, especially in the case of strong frequency parameters.

During the deceleration phase of a pulsated flow, when the stationary component is not too large compared to the time-dependent component, the fluid movement close to the wall is reversed compared to the fluid displacement direction in the tube section centre. The reverse flow is more pronounced near the convex wall. The shear stress close to the wall varies in the absolute value and in direction.

The superposition of oscillatory on stationary flow is of strong interest in the cardiovascular field in investigating problems in blood circulation and vascular ageing. Rabadi et al. [1980], in an analytical study of pulsatile flows in curved pipes with small curvature radius, observed that the amplitude of shearing forces decreases with increasing frequency. Moreover, a considerable variation in secondary flow intensity occurs at small frequencies of oscillation during a pulsation cycle.

Through experimental measurements of the axial and secondary velocities in a $180\,\mathrm{deg}$ curved pipe, Talbot and Gong [1983] highlighted the existence of reverse flows at the inside wall during the deceleration phase. The reverse flows and the appearance of the vortex were highlighted numerically by Toshihiro et al. [1984], who observed that the secondary flow is characterized by more than two vortex pairs. Chang and Tarbell [1985] found that the secondary flow is characterized by only one vortex pair at the beginning of the deceleration processes. In the half-phase of deceleration, the secondary flow becomes complicated with the appearance of a new vortex pair near the outside wall that disappears

with the start of the last third of the deceleration phase, only to reappear at the end of the acceleration process. More recently, Hamakiotes [1988] studied the effect of the Reynolds number on pulsatile flow in uniformly curved pipes and found that the secondary flow becomes much more complicated with increasing average stationary Reynolds number.

All things considered, then, pulsatile flows in uniformly curved pipe remain much more complicated than the straight tube or steady Dean flows. The fluid motions resulting from the pulsations have been found to depend on the characteristic oscillation parameters. In spite of extensive and concentrated efforts since the early 1970s, the theoretical and experimental investigation of pulsatile pipe flows is far from complete.

1.3.4 Theoretical and experimental models on tapered tubes

The need to capture the nature of the arterial tree and define its physical properties in order to use them as the correct parameters in modelling, have lead to investigation of the geometrical tapering of the tubes. Young [1808], was one of the first to mention possible effects in the blood circulation. Taylor [1965] was concerned with wave propagation in a non-uniform transition line.

Wemple and Mockros [1972] solved a one dimensional non-linear mathematical model by the method of characteristics. This non-linear model included geometric and elastic taper of the flexible tube. They compared their model with data measured in humans. The elastic taper theoretically affects the wave transmission and reflection in the same way as to that of geometric taper. The degree of the elastic taper is small compared to that of the geometric taper, therefore they concluded that the elimination of the elastic taper does not have significant effects on the model. The geometric tapering on the other hand is quite important for the presence of reflection waves. They concluded that the system behaves in a linear way for the lower frequencies, while for the higher frequencies the non-linearities are important. The linear theory is unable to deal with tapered tube if the pressure pulse is high.

Belardinelli and Cavalcanti [1992] used a two dimensional non-linear model. They point out that the natural tapering of the arteries should be taken into account as it has been indicated from in-vivo measurements. Their model encompasses the motion of a pulse-driven viscous fluid in a geometrically tapered flexible tube. They make the assumption of uniform pressure in a cross section. Their results show that the tapering does not influence the wave velocity but it influences the waves' attenuation rate. They used infinite extremity impedances to maximally enhance the reflections so that the overall attenuation is only due to arterial properties and in particular the natural tapering. The natural tapering causes a continuous increase in the pulse amplitude as it moves from one side of the tube to the other. In a 0.6m long tube with taper angle of 0.1 the pulse amplitude at the end of the tube is more than twice the input pulse. The reflected pulse is greatly damped and its shape is quite different from that of the direct pulse.

Einav et al. [1988] used an LCR (inductance-capacitance-resistance circuit) electrical analogue to study wave propagation in exponentially tapered tubes with main interest in reflections at bifurcations Their model was compared with the one of Westerhof et al. [1969]. They concluded that the input

impedance is low for high frequencies. Therefore, blocked branches in the vicinity of the heart do not significantly contribute to the input impedance. More distal bifurcation, such as the ileac bifurcation, can affect the input impedance at low frequencies. From their reflection condition they conclude that in order to maintain continuity in a junction, the characteristic impedance and peripheral impedance are doubled and the cross-section of the branches is 15% larger than the main branch.

Chang et al. [1994] used the electrical analogue in which they included the non-uniform properties of the tube, as well as the geometric and elastic tapering. They compared their model with in-vivo measurements in dogs. They found good agreement between their impedance parameters derived by their non-uniform model and the ones measured in the animals.

Fogliardi et al. [1997] used an exponentially tapered electrical analogue to model descending aortic circulation. In their model they used five parameters to characterize the input impedance: the characteristic impedance, the compliance of the tube, the tube length, the time constant of the load and the peripheral resistance. They performed open chest in-vivo measurements in dogs to obtain pressure and flow measurements. From the comparison of their model with the in-vivo data they found that the tapered tube models showed a slightly closer matching with the experimental flow and the reproduction of the input impedance.

After a thoroughly survey of experiments performed with tapered tubes, a vast amount of literature of in-vivo measurements in humans and animals was found but only two papers studying wave propagation in geometrically tapered elastic tubes: von Kries [1892] and Reuderink et al. [1988].

von Kries [1892] was interested in understanding blood pressure waves. He was the first one to perform experiments on a rubber tapered tube. He had two straight tubes of 22 mm and 5.5 mm diameter connected to each other by a 140 mm long conical part. His interest was to use tapering to eliminate the wave reflections of a pressure wave form when transmitted from a tapered tube to a straight one.

Reuderink et al. [1988] used a uniform latex tube 0.5 m long with 12.73 mm outer diameter and thickness 0.14 mm with a variation of ± 0.01 mm for the straight tube; the tapered one varied from 15.88 to 9.45 mm outer diameter (46 degree taper) with horizontal to vertical slope of 0.008 and thickness 0.13 mm ± 0.01 mm. The tubes were manufactured by dumping the mould in latex rubber. The working fluids used were salt solutions of different concentration and glycerin solution. The salt solutions were used in order to be able to measure electromagnetically the flow. A pneumatically driven piston was used for the pulse initiation. Impulse or sine waves were used for the excitation. The sine wave did not produce a steady flow component. A catheter tip manometer was used for measuring the pressure at different positions along the tube.

They compared the real part of the true propagation coefficient with the apparent damping and the damping coefficient calculated from the Womersley theory. They also compared the true phase velocity with the measured apparent phase velocity, foot-to-foot velocity, and calculations of phase velocity parameters using the Womersley's theory and the Moens-Korteweg equation. From their comparison they conclude that the three point method used to obtain the propagation coefficient is in agreement with all other estimate for a uniform tube. For a tapered tube the three point method causes an error estimation

of the propagation coefficient. They state that in their experiments tapering only cannot take account for the differences between in-vivo measurements of the propagation coefficient using the three-point method and calculations based on the Womersley's theory since in their results taper caused a discrepancy only at these frequencies the damping was largely underestimated instead of overestimated.

Blood flow analysis is a very complex physical phenomena and modelling all its intricacies can easily become an herculean task. One must thus learn to make some simplifications while keeping in mind that those will have to be verified. Unfortunately and due to the complications mentioned before most of the results of computational experiments are limited to previously existing experimental or computational results for validation purposes.

Some limitations are found with experimental measurements. For instance *in-vivo* experiences requires a careful handling of the subject, specific conditions of measurements, law restrictions, etc. Experimental rigs, on the other side, are limited on the quantities of interest that can be measured and are difficult to reproduce exactly. This can be due to special conditions or due to the instruments used to measure a quantity.

The most predominant theoretical model with many improvements in wave propagation in flexible vessels is the one postulated by Womersley. His theory, for tethered or non-tethered tubes, has been experimentally validated with the works of Klip [1962] and Gerrard [1985]. These were verified beyond the entry length. For finite length tubes countless theoretical models and experimental data have proved its accuracy.

Even so many quantitative questions have yet to be answered in wave propagation. The prediction of pressure wave velocity is correctly made by using the linear theory as experimental and *in-vivo* measurements have proven. The damping of the arterial pulse along the tube is not so correctly represented. Reflections appear due to the closed ends and so affect the measured pulse.

Discrepancies are also present due to physical non-linearities, which are not modelled correctly. The arterial system is geometrically and thermodynamically non-uniform. Variations on the cross section geometry, compliance and branching are not taken into account.

These non-linearities appear due to the dependency of pressure on the factors previously mentioned. Geometric and elastic tapering play a fundamental role in the arterial system. Because of tapering, local compliance of blood vessels decreases as their position is further away from the heart, while the characteristic impedance increases. Wemple [1972] believed that even with the non-linearity behaviour inherent to the system, if lower frequencies were to be applied (around 80 beats per minute) linear behaviour simplification could be assumed without losing much accuracy.

In order to assess the importance of non-linearities and before making any assumptions upon the necessity to take them into account or not, quantitative agreement between experiments and measurements must be achieved. Thus the importance of well planned experiments. Some theoretical models do take into account those non-linearities of the arteries. The problem with those models is that their validation is limited to *in-vivo* measurements, which makes their accuracy and conditions deeply difficult to assess. Literature states that there is insufficient data for non-linear tubes. The work of von Kries [1883] and Reuderink et al. [1989] took into account geometric non-linearities and flexibility.

The elastic taper affects the wave transition and reflection in a similar form as geometric taper. The degree of elastic taper is small relatively to the geometric taper. Geometric taper is thus an interesting situation to investigate wave propagation.

1.4 Objectives

With this thesis we are interested first and mostly on establishing a working procedure for FSI simulations using STARCCM+ software. With this objective in mind we want to be able to observe the following phenomena:

- the tube deformation and buckling mode.

- the pressure wave propagation.

- the effect of elasticity on the pressure/velocity field and the wall shear stress.

- the secondary flow development and fluid instabilities.

- the effect on the flow properties and the solid deformation when a change in elasticity occurs.

In a first stage we will simulate and compare our results against the existing literature. As it is obvious one cannot guarantee the accuracy of the simulation for every possible situation. In order to obtain sound results which would validate our model the articles selected focus on a certain property we wish to assess. For example the degree of solid deformation. This allowed to test different numerical methods, which in turn allowed us to better understand the results obtained and to tune up the model in order to obtain a realistic result.

Henceforth to obtain secondary flow we proceed to study the effects of elasticity in a bend pipe. We use another article to perform comparison and verify the results.

With the knowledge accumulated with these three simulations we proceed to a case where all the aforementioned phenomena are present, the blood circulation in the aorta. A simplified model of the aorta is made with the addition of taper which will introduce a local reinforcing of the rigidity of the tube and the ramification arteries are removed. The Figure 1.1 shows the flow configuration for the main topic of the present research. With this study we will be able to push the simulation to the limit and truly assess the effects of 3D in FSI. A final discussion of the results obtained and future work aspects is done.

Last but not the least, the numerical work is also motivated by the need to understand further the flow mechanics in fluid-structure applications and how the elasticity parameter factors in each one of the previous control parameters. In literature there are many questions that have not yet been satisfactory

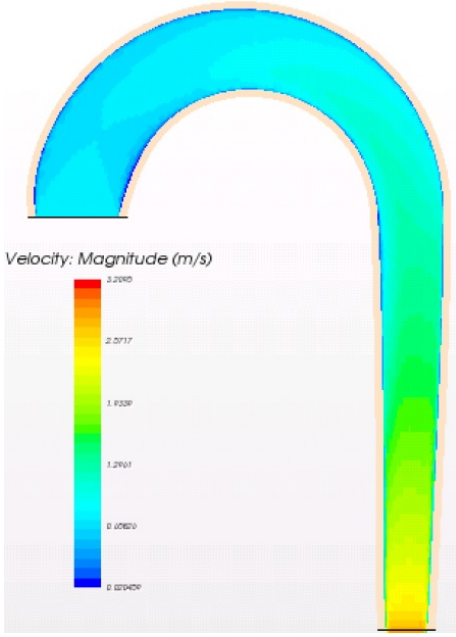

Figure 1.1: Flow configuration for present configuration.

answered. The effects of geometric taper and elasticity that are present, for instance, in the arterial tree morphology. The main reason for this is the apparent limitation of *in-vivo* measurements in combination with the lack of well defined laboratory experiments in the literature. Thus, there is a need for developing numerical models which would allow, with the existing experimental results, to help to validate and enhance the tools available to further understand and correctly assess these phenomena.

1.5 Outline of the thesis

In Chapter 2 the main physical aspects which are relevant for this thesis will be presented along the with the numerical methods which validate our model. In Chapter 3 we present the results of our main research topic, blood flow in aortic artery, along with a validation case for a 90 degree bend pipe. In chapter 4 the conclusion of our findings are presented, along with the main achievements and suggestions for future work in this field.

Chapter 2

Physical and Numerical Models

In this chapter the fundamental theory and equations that characterize the physics that involves FSI will be briefly presented. The main variables that are used to solve the equations for a Hookean solid and a Newtonian fluid are typically the displacement, velocity and pressure field. This approach is used because the stress tensor in solids is defined in terms of displacement and in fluids in terms of velocity and pressure. This is quite useful since we can correlate these variables directly without the use of other variables. Now we need to reformulate the solid equations so that they take into account an unknown velocity and pressure.

2.1 Governing Equations

The behaviour of solids and fluids can be described by the same continuity and momentum equations since they are both continua. No simplifying assumptions are made for the momentum and continuity equations for fluids and solids and both are considered as compressible. The difference is found with the constitutive laws. In this thesis we will assume linear elastic (also known as Hookean) solid and thus the constitutive law is based on a stress-strain relationship. For the fluid we will be using both linear viscous (Newtonian) and non-linear (Non-Newtonian) fluids.

2.1.1 Equations: Solid Mechanics

The subject of study of solid mechanics is the deformation, strain and stresses that occurs in the solid materials. In fluid structure interaction we are mostly interested in the deformation of the solid, for instance in a collapsible tube or the wave propagation in a pipe. The concepts below are thus of the utmost importance when studying cases where the coupling of fluid and solid is so strongly felt.

2.1.1.1 Stress

Stress is the measure of an internal force divided by the area over which the force is applied, with the area tending to zero.

$$\sigma = \frac{F}{A} \tag{2.1}$$

A full tensor description is necessary for taking into account all the stress components at a given point on any plane. It can be written in matrix or in a vector form.

$$\sigma = [\sigma_{xx}\sigma_{yy}\sigma_{zz}\sigma_{xy}\sigma_{yz}\sigma_{zx}]^T \tag{2.2}$$

Since the sum of moments must go to zero at an infinitesimal point, the stress tensor is symmetric:

$$\sigma = 0 \tag{2.3}$$

In the literature it is common use to refer to the diagonal terms as the normal stresses, since those act on the normal face of the element. The other terms are also known as the shear stresses.

We can obtain the traction stress by multiplying the shear tensor by the normal of a given plane.

$$\tau = \sigma \bullet n \tag{2.4}$$

This equation is knows as the equilibrium equation. For every body there is a plane where the shear stresses are zero with only the normal stresses remaining. When such situation arises we obtain what is known as the principal stresses $\{\sigma_1\sigma_2\sigma_3\}$. They are written in order of magnitude, thus making $\sigma_1 > \sigma_2 > \sigma_3$.

The principal stresses are also the eigenvalues of the stress matrix. The use of Mohr circle to describe the principal stresses in two dimension is also very common.

2.1.1.2 Deformation

The deformation of a part is defined by a vector quantity which describes how much a material point on the part is deformed or displaced from its original configuration. A given point can be characterized in terms of deformation as a function of $x = x_0 + u(x_0)$, where $u(x_0)$ is known as the displacement field.

2.1.1.3 Strain

Strain is the measure of how much a body deforms. If two material points on an undeformed body are originally at a distance of l_0 and in some deformed configuration the two points are now located at a distance l, the strain ε is measured as:

$$\varepsilon_G = \frac{(l - l_0)}{l_0} \tag{2.5}$$

ε_G is known as the Green strain. As for stress, to completely describe strain at a point one requires a tensor. For small strains the relationship between the deformation and the strain is given by:

$$\varepsilon = \frac{1}{2}(\bigtriangledown u + \bigtriangledown u^T) \tag{2.6}$$

This equation is one of the constitutive equations that is required to model the solid. The other one is obtained by expressing the relationship between stress and strain. For all the case studies where there is a solid involved, it is assumed that it obeys a linear isotropic elastic behaviour. This results in the following equation known as Hook's law:

$$\sigma = C\varepsilon \tag{2.7}$$

where C is the stiffness tensor. This is the second constitutive law necessary to solve the solid mechanic aspect of the problem.

With the momentum Eq. (2), the equilibrium Eq. (3) and the two constitutive Eqs. (5) and (6), the overall structural behaviour is now completely described.

2.1.1.4 Finite Volume Stress Analysis Methodology

The process by which the wall deformation is calculated is done according to these steps. Taking the differential form of the solid momentum equation:

$$\rho\ddot{u} = \bigtriangledown \bullet \sigma + b \tag{2.8}$$

where b is the body force, and a general constitutive law between the stress tensor and the strain tensor:

$$\sigma = \sigma(\varepsilon, T, k) \tag{2.9}$$

where T is the temperature and k represents other internal variables. Also since small strain is assumed we can use Eq (5) to characterize strain. The finite volume form is now determined by the integration of parts to obtain:

$$\int_V \rho\ddot{u}dV = \int_A \sigma dA + \int_V bdV \tag{2.10}$$

The acceleration terms can be modelled either using a 1st order (Backward Euler) or a 2nd order (Newmark). In STAR-CCM+ the large displacement model is also included since the displacement can be as large as the cell size.

2.1.1.5 Rayleigh Damping Methodology

During a numerical simulation where the structural behaviour is analysed, there can be a lack of either physically real or unwanted numerical damping. To try and solve this problem the Rayleigh Damping methodology is used. The damping is written as:

$$C_r = \frac{M}{\tau_M} + \tau_K K \tag{2.11}$$

where C is the viscous damping matrix, M is the mass matrix, K is the stiffness matrix, $\frac{1}{\tau_M}$ is the mass damping coefficient, and τ_K is the stiffness damping coefficient. In the finite volume stress analysis the stiffness matrix is not computed, instead an equivalent law for viscous stress is used:

$$\sigma_d = 2G\dot{\varepsilon} + \lambda tr(\dot{\varepsilon})\delta \tag{2.12}$$

where $\dot{\varepsilon}$ is the rate of change of the deformation rate gradient. The total stress is given as the sum of the elastic and viscous damping parts and with an elastic model with pseudo strain of the form:

$$\tilde{\varepsilon} = \varepsilon + \tau_K \dot{\varepsilon} \tag{2.13}$$

the elastic model returns the total stress due to both the elastic and viscous damping.

2.1.2 Equations: Fluid Model

The fluids used during the simulation can be assumed as incompressible, under such hypothesis the Navier-Stokes equations are given as:

$$\frac{\partial \rho}{\partial t} + \frac{\partial \rho U}{\partial x} = 0 \tag{2.14}$$

$$\frac{\partial U}{\partial t} + u \bullet \bigtriangledown U = -\frac{\bigtriangledown P}{\rho} + \nu \bigtriangledown^2 u \tag{2.15}$$

where ν is the kinematic viscosity, U is the velocity of the fluid, P is the pressure and ρ is the fluid density. The Eq. 2.14 is known as the continuity equation and Eq. 2.15 as the momentum equation.

Since the fluid is viscous and incompressible, the following constitutive equation is used:

$$\tau_{ij} = 2\mu s_{ij} \tag{2.16}$$

which relates the stress tensor τ_{ij} and the strain rate tensor s_{ij}, μ is the dynamic viscosity of the fluid. The strain rate tensor is defined as:

$$s_{ij} = \frac{1}{2}(\frac{\partial U_i}{\partial x_j} + \frac{\partial U_j}{\partial x_i}) \tag{2.17}$$

The solving methodology is done with a segregated solver which can be described as using a col-

located variable arrangement and a Rhie-and Chow-type pressure-velocity coupling combined with a SIMPLE-type algorithm. For boundary conditions the no slip condition is applied at the wall.

2.2 Similarity parameters

There are many geometries involving fluid structure interaction, furthermore in order to replicate some phenomenon within laboratory limits there is a need for a set of dimensionless parameters which allow to replicate the same circumstances. In this area the parameters that are necessary to define are: the Reynolds number, the Dean number and the Womersley number.

2.2.1 Reynolds number

The Reynolds number, Re_D, in an internal flow of mean sectional velocity U within a pipe or vessel with a characteristic diameter D is defined as

$$Re_D = \frac{\rho U D}{\mu} \tag{2.18}$$

where μ is the dynamic viscosity of the Newtonian fluid. This dimensionless number makes a typical appearance in the Navier Stokes equations. It's physical meaning can be interpreted as the ratio of inertial forces to viscous forces. This is easily seen if we rewrite the definition in the following form

$$Re_D = \frac{\rho U D}{\mu} = \frac{\rho U^2}{\frac{\mu U}{D}} \approx \frac{Mom.flux}{wallshearstress} = \frac{inertialforces}{viscousforces} \tag{2.19}$$

In the first deduction the Reynolds number can be interpreted as a ratio of the momentum flux ρU^2 over the pipe, i.e. momentum ρU crossing the diameter at speed U, to $\frac{\mu U}{D}$ which is an estimate of wall shear stress. Since inertial flux is related to the concept of an inertial force, we can argue that Reynolds number is a measure of inertial forces to viscous forces. When Reynolds number is large the inertial forces are dominant over viscous forces and vice versa. Therefore the Reynolds number is a useful parameter in order to identify the flow transition of laminar regime to a turbulent one.

2.2.2 Dean number

This parameter appears when dealing with curved planar pipes, the Dean number, De, is thus defined as

$$De = 4\sqrt{\frac{D}{R_c}} Re_D \tag{2.20}$$

where R_c is the radius of curvature, D is the pipe diameter and Re_D is the Reynolds number based on mean velocity and diameter. Dean number can be interpreted physically as the balance between the forces due to inertia and centripetal acceleration and the viscous forces.

$$De = 4\sqrt{\frac{D}{R_c}}Re_D = 4\sqrt{\frac{\rho\bar{R}_c\frac{U^2}{D^2} \times \rho U^2}{\mu U}D} \approx \frac{\sqrt{centripetalforces \times inertialforces}}{viscousforces} \tag{2.21}$$

in the above equation the term $\bar{R}_c = \frac{R_c}{D}$ and the term $\rho\bar{R}_c\frac{U^2}{D^2}$ is an approximation of the force to produce centripetal acceleration since $\frac{U}{\bar{R}_c}$ is a measure of the angular velocity.

2.2.3 Womersley number

When dealing with unsteady flows the most common flow parameter is the Womersley number, W_o, defined as

$$W_o = \frac{D}{2}\sqrt{\frac{2\pi}{\nu T}} \tag{2.22}$$

where $\nu = \frac{\mu}{\rho}$ and T is the fundamental period of the oscillatory flow. The physical interpretation of the Womersley number is as the ratio of pipe diameter to the laminar boundary growth over the pulse period

$$W_o = \frac{D}{2}\sqrt{\frac{2\pi}{\nu T}} \propto \frac{D}{\sqrt{\nu T}} = \frac{Diameter}{Bound.lengthgrowthintimeT}. \tag{2.23}$$

2.3 Pulse Wave Velocity

Pulse wave propagation can be described as an arterial wall disturbance caused by the ejection of the blood from the heart that propagates mainly toward the periphery. The diagnosis of cardiovascular disease by measuring pulse wave velocity (PWV) is believed to be a promising technique. The PWV is defined as the velocity of an arterial wall disturbance toward the periphery, which occurs, for example, due to contraction of the ventricle. In general, the PWV is determined by measuring the time delay of the waveforms, Δt, between the two sites with a known distance *L*. Therefore,

$$PWV = \frac{L}{\Delta t}. \tag{2.24}$$

the PWV is believed by clinicians to be increased with the severity of vascular disease such as atherosclerosis. The concept for applying the PWV as an index of vascular disease is based on the Moens-Korteweg equation, which formulates the PWV of a long straight elastic tube. According to the

Moens-Korteweg equation,

$$PWV = \sqrt{\frac{Eh}{2\rho r_i}}, \tag{2.25}$$

where E is the Young's modulus of the arterial wall, h is the wall thickness, ρ is the blood density, and r_i is the internal radius of the artery. For thick-walled tubes, the Moens-Korteweg equation has been modified by computing the strain on the middle wall of the tube.

$$PWV' = \sqrt{\frac{Eh}{2\rho(r_i + \frac{h}{2})}}. \tag{2.26}$$

In the presence of flow, it is assumed that the wave will be convected with the cross-sectional averaged velocity of the blood. For a thick-walled tube with flow, we therefore use the ``modified Moens-Korteweg equation ´´,

$$PWV'' = \sqrt{\frac{Eh}{2\rho(r_i + \frac{h}{2})}} + U. \tag{2.27}$$

Where U is the cross-sectional averaged velocity of the blood. It is recognized that an increased Young´s modulus *E* will result in an increased PWV. This interpretation, however, is not always applicable to living blood vessels because the Moens-Korteweg equation includes some assumptions that are not valid for human blood vessels. The Moens-Korteweg equation is valid only when an infinitely long, straight and mechanically as well as geometrically homogeneous tube whose wall is very thin is filled with a still, non-viscous fluid. In a real artery, however, the anatomy and the constitution of the blood vessel differ from place to place, therefore, the mechanical properties of the arterial wall depend on its regional position. Moreover, the geometry of the blood vessel is not infinitely long and straight but distributed complicatedly in a three-dimensional space, including many branches, curved regions and tapering toward the periphery. In addition, the blood is not stationary but flows with its velocity changing in time and space. Hence, the diagnosis of cardiovascular disease by measuring PWV, which relies on the Moens-Korteweg equation, is not correct in the strict sense. The measured PWV of the human blood vessel is a result of several superimposed factors which influence each other, and are not so simple that the Moens-Korteweg equation can be applied. Therefore the use of these expressions when calculating the pulse wave should be done with some measure of caution.

2.4 Numerical Mesh

In computational fluid dynamics one of the most important parts that precedes the processing part of the simulation is the mesh rendering. In Finite Element as in Finite Volume methodologies we must ensure

that for a particular domain that we have enough elements or faces to be able to make an accurate calculation. Two very important factors have to be taken into account. One is cell geometry type and its' position along the geometry and the other is the cell refinement in the body.

It is easy to understand, in Finite Volume, why it is different to use a triangular mesh or a polyhedral mesh. In our cases we will be dealing exclusively with pipes that have a circular cross-section. A triangular mesh cannot be applied without having some slight misalignment along the circular walls, while the polyhedral mesh can more easily fit in such a geometry. This will allow for a better alignment of the cells in relation to the fluid or the solid part, which in turn will minimize errors due to transverse calculations. For example let us imagine a circular cylinder, if the mesh is aligned with the flow path, then velocity calculations (for instance) will be calculated correctly along the respective axis and will not suffer from truncation errors.

Another very important part of the meshing phase is how refined should be the mesh for a given situation. Here it is very difficult to establish a rule since this will be due to the geometry, the parameter of interest that we wish to compute and with how much computational power we have available for the given simulation. Ideally one who is acquainted with the physical phenomena that will be reproduced is able to make an educated guess to where he or she should apply the refining. Sadly that is not the case when doing investigation work or when the parameter of importance is present in a very long area.

In our case the first problem can be quite easily solved by recurring to polyhedral meshing with the generalized cylinder who will generate a sort of structured mesh. We present in the Figure 2.1 the meshes used in two different cases. In the left side we see the pressure wave propagation situation and in the right side the $90°$ bend pipe case.

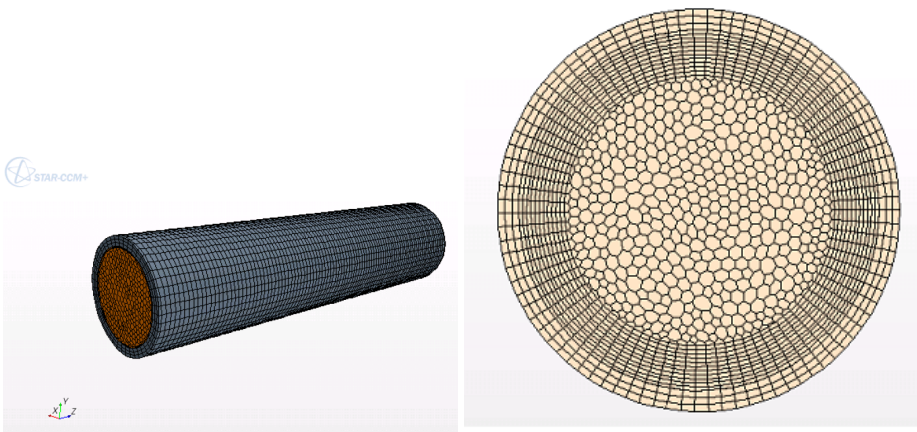

(a) pressure wave propagation mesh (b) 90 degree bend mesh

Figure 2.1: Pressure wave and 90 degree bend pipe meshes.

The cell alignment is ideal not only to the fluid flow in the tube but also in relation to the applied forces. Indeed we know that the flow will mostly have an axial component while forces such as pressure will be acting in a radial component.

Now the second problem cited above is not so simple to solve. We have found out that there is a great variation of what would be called as an ``optimum refinement ´´. Since in the straight collapsible tube we

wish to compute a very detailed and extensible deformation process we need to increase considerably the refinement of the mesh. Otherwise we would rapidly see the appearance of distorted cell which would result in a fatal error. Thus the cell refinement has taken us to the point where we have a count of around 800000 cells total (see Figure 2.2). This is immense when considering the type of problem we want to solve and how fewer cells we would have required, if say, we were to assume an initial undeformable buckling geometry. When fewer cells were used, around 200000, we would only reach a total deformation of $\approx 60-70\%$ of the target deformation. When using the more refined mesh the margin of error came to a mere 3%. It is very clear that mesh refinement plays a major role in the results that are obtained. Of course we do not affirm that our meshing was the most optimized one but everything was done to minimize the cell count in each situation.

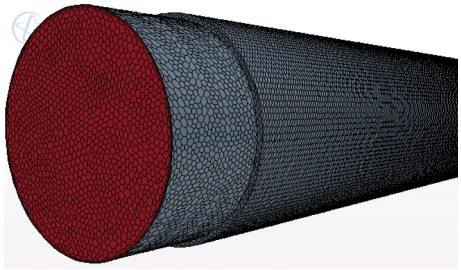

Figure 2.2: Straight collapsible tube mesh.

Table 2.1: Mesh Validation

	Collapsible tube
mesh 1	200000 cells (up to 500000 cells), 25 [%] error and 10E-6 residual
mesh 2	800000 cells, 3 [%] error and 10E-8

Table 2.2: Mesh Validation

	Pulse wave propagation
mesh 1	80000 cells 8.5 [%] error and 10 power-6
mesh 2	160000 cells 8.45 [%] error and 10 power-6

2.5 Numerical Validation

In this section we present the two cases that were selected to validate my model with fluid-structure interaction effects. While we cannot say that a thorough validation was done, which would require a too great number of tests, we choose relevant articles published in renown journals for the situations in which we are interested.

2.5.1 Straight Collapsible Tube

The first case is taken from Marzo et al. [2005]. The test case consists of two straight tubes with a fixed Reynolds number and a constant external pressure field. According to the paper the deformation of the

tube goes as high as 86.4% flattening in both situations. This is a very high deformation which will put to the test the capabilities of the simulation in terms of FSI. This example was considered a suitable trial and would serve as a first validation case. Table 2.3 lists the main parameters of test case 1.

Case	**1**	**2**
Solid Properties		
Radius (R)	4 [mm]	4 [mm]
Length (L_{up})	R	R
Length ($L = L_{down}$)	10R	10R
Thickness	$\frac{R}{20}$	$\frac{2R}{20}$
Density	2702 [Kg/m^3]	2702 [Kg/m^3]
Young Modulus	3 [MPa]	3 [MPa]
Poisson Coefficient	0.3	0.3
Fluid Properties		
Reynolds number	350	350
Physical conditions		
Pressure	520 [Pa]	1550 [Pa]
Rayleigh Damping		
Mass damping coefficient	-4.73944 [Hz]	-10.0338 [Hz]
Stiffness damping coefficient	8.84E-4 [s]	8.58 [s]

Table 2.3: Properties for the straight collapsible tube.

As we can see in Table 2.3 we have a simulation which could be classified in solid mechanics as thin shell and another as thick shell. The difference between both cases is that suitable simplifications can be done when solving the solid equations. Testing both situations will allow to have a better grasp of the capabilities of the solid solver.

The meshing of the pipe proved to be very heavy, with more than 800.000 cells, and would reveal to be one of the major difficulties of this case. When running the simulations both encountered a ``volume problem ´´in which some cells of the solid where not correctly solved in the final phase. In order to break through this problem the simulation was stopped at a previous time and the surface mesh was extracted and opened in another simulation. Then a volume mesh was done and since it possessed less cells we were able to successfully reached stable conditions. This problem can easily rise since convergence of a buckled state is extremely hard due to the tube buckling mode being highly responsive to pressure fluctuations, even if small. This was also expected since the authors also had the same problem as we did.

We successfully obtained a degree of collapse of 86.4% of the radius. The resulting shape deformation is, as expected, different for each situation,Figure 2.3, Figure 2.4. Now a major difference that is clearly seen in Figure 2.4 is the rotation that occurs in the thin tube. The deformation continues to be symmetric however there is the possibility for some rotation in the deformation. The reason for this comes from the evolution of the oscillations present in the tube during the buckling process. In fact the tube starts buckling according to a axisymmetric state. When the oscillations grow in amplitude beyond a critical value, there is a chance that, in conjunction with the flow, a sloshing effect arises and the tube will respond by alternating it's major and minor deformation axes. When these oscillations start to decay, then we see a stabilization of the axis with a slight rotation.

The error (of deformation) obtained with the thinner mesh refinement was of 0.32% for the thin tube

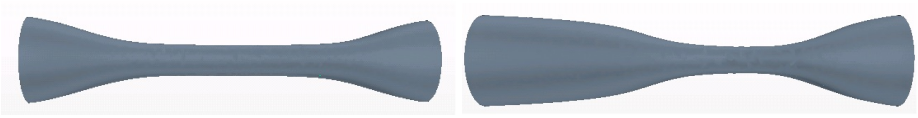

(a) Thin tube (b) Thick tube

Figure 2.3: Resulting deformation, lateral view.

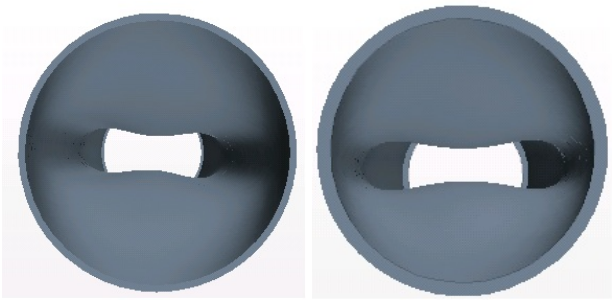

(a) Thin tube (b) Thick tube

Figure 2.4: Resulting deformation, front view.

and of 0.18% for the thick tube. The error for the location of maximum collapse was well under 3% for both cases. The results are thus in good agreement with the ones observed in Marzo et al. [2005]. We can thus conclude that even with the model not using the shell theory for the solid, we are still capable of replicating numerical results from recognised scientific sources.

2.5.2 Pressure Wave Propagation in a Straight Tube

When we have a pulsatile flow inside a tube there is also a wave propagation on the solid wall. In effect since there is a change in the pressure gradient, a pulse wave will propagate originating a change in the wall displacement which travels also along the tube wall. This phenomena is very difficult to simulate in a numerical experiment due to the high travelling speed that require a very small time step. This can sometimes result in numerical errors arising from the inability of the system to calculate a steep acceleration, despite the actual deformation being small. Adding to this the need to couple the displacement of the tube with the fluid reaction and vice versa, the task can quite easily become near impossible with the oscillations. Our test case is taken from Janela et al. [2010] and table 2.4 sums up the main aspects of the simulation.

In Figure 2.6 we can see both the geometry and the mesh used in the simulation.

In this simulation we are, as was the case in the previous case, interested in the deformation behaviour of the wall. The results obtained are shown in Figure 2.7

There are differences between the results obtained our simulation and the one in Janela et al. [2010] (2.7). Although we managed to obtain the same magnitude in the deformation we can see that our wave propagation seems to travel slightly slower (difference of 3 ms) than the one from the literature and also the reflection presents a different behaviour. In our simulation the pressure wave is much more attenuated and the reflection is much weaker than in the paper. This would lead us to believe

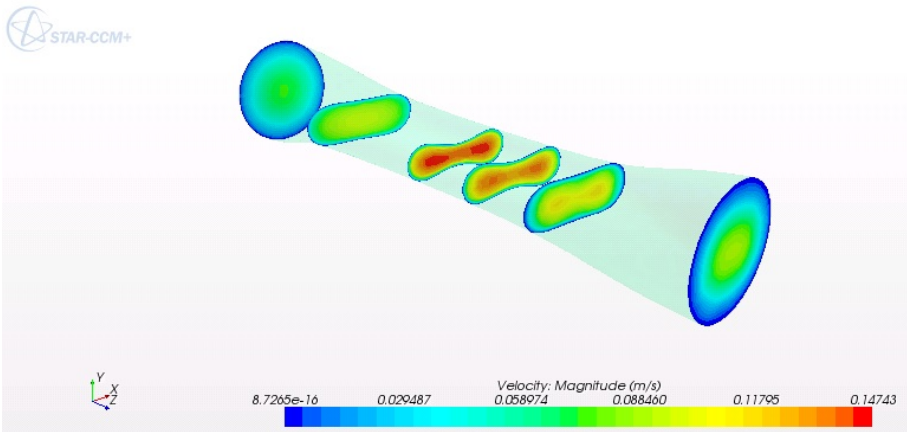

(a) Thin tube

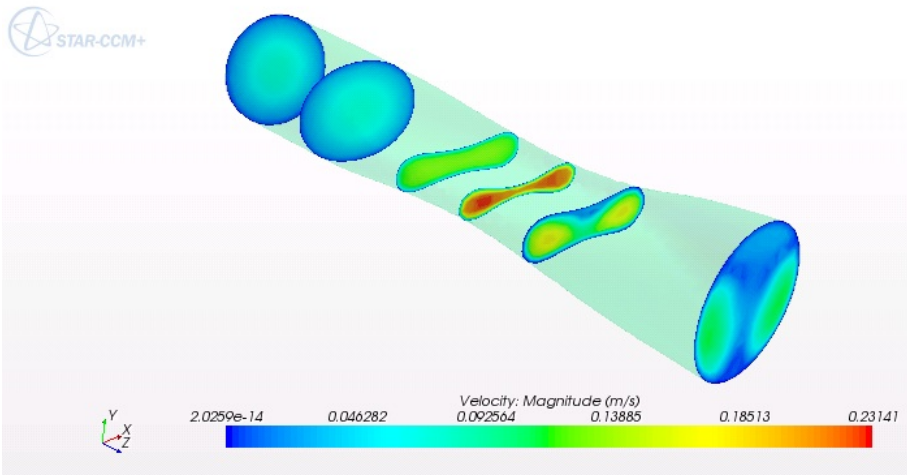

(b) Thick tube

Figure 2.5: Velocity in different sections along the tube.

Table 2.4: Summary of case from Janela et al. [2010]

Case	
Solid Properties	
Radius (R)	0.5 [mm]
Length (L)	5 [cm]
Thickness	0.1 [cm]
Density	1150 [Kg/m^3]
Young Modulus	0.3 [MPa]
Poisson Coefficient	0.3
Fluid Properties	
density	1050 [Kg/m^3]
dynamic viscosity	0.004 [Pa-s]
Physical conditions	
Pressure max	1666 [Pa]
Rayleigh Damping	
Mass damping coefficient	-4.00687 [Hz]
Stiffness damping coefficient	0.001476 [s]

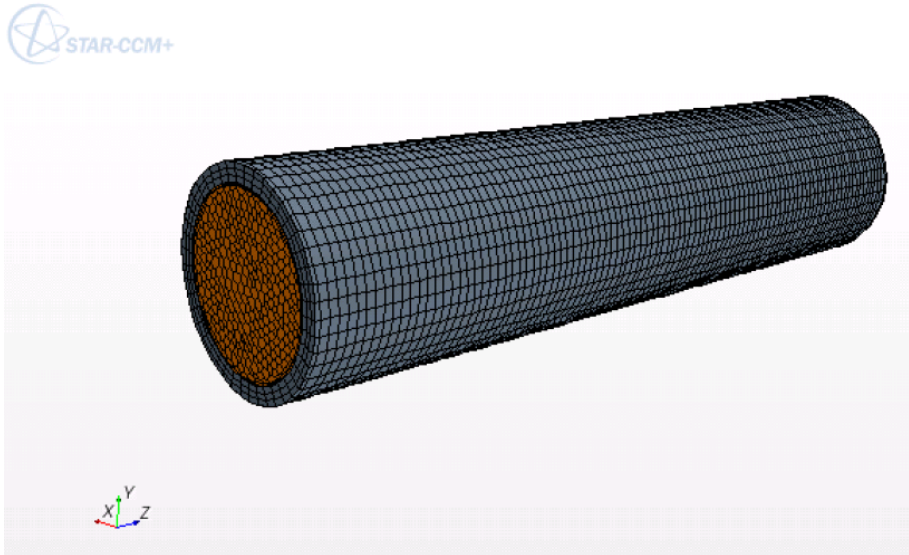

Figure 2.6: Tube Geometry

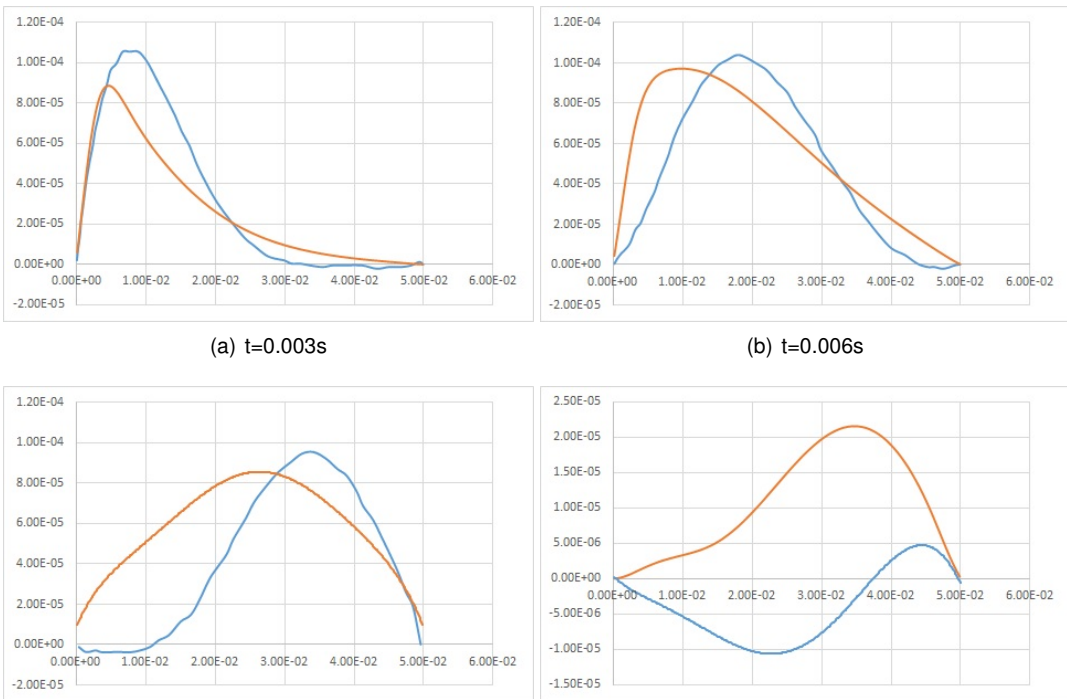

(a) t=0.003s

(b) t=0.006s

(c) t=0.009s

(d) t=0.012s

Figure 2.7: Resulting deformation (amplitude in y axis and length in x axis) for t=0.003s, t=0.006s, t=0.009s and t=0.012s (blue - Janela et al. [2010] orange - simulation).

that the boundary conditions imposed are able to absorb the incoming wave which would be physically realistic. In truth wave reflection obtained in numerical results have been proved to be superior to the ones obtained in laboratory. The difference between our cases can arise from a series of factors or all of them combines. From the fact that the solid equations are not taking into account that the solid is not isotropic, the boundary conditions being fixed in one case and damped in the other one, etc... Differences in behaviour are thus bound in appearing. It is important that the results observed denote

a more conservative approach since the young modulus is equal for any direction and thus we may say that our model has a higher rigidity than the one from Janela et al. [2010].

The results obtained in this section show that up until the reflection we obtain the same wall response to the propagation wave, with a slight temporal delay. The obtained reflection is however much lower (up to 50% less) than the one from the literature. It is assumed that software code and solid models are responsible for these discrepancies. Since a conservative result is observed we deem that the simulation has given acceptable results.

Chapter 3

Results

In this section we present the two cases that were selected to analyse FSI effects. The first case is the flow through a 90 degree rigid or elastic curved pipe where we aim to compare the differences in secondary flow arising from pipe deformation. The second configuration is an idealized tapered aorta artery.

3.1 Flow through a 90° Curved Pipe

3.1.1 Flow through a 90° Rigid Curved Pipe

Up until now we have been studying what happens to a set geometry and its' internal flow if the elasticity of the tube is to be taken into account. Although many interesting phenomena have been seen, such as the self-sustained oscillations or the pressure wave propagation, this is only a mere fraction of what happens in the daily world. In reality when one studies pipes, from engineering to biomedical applications, most of them have some degree of curvature. This change in geometry is not as trivial as one would think at first sight. As we saw in Chapter 2 the flow changes its' behaviour drastically. Furthermore the change from a steady flow inlet boundary condition to a pulsatile flow will make it so that we will not obtain a single steady flow behaviour. Thus to truly come to understand what happens when dealing with such configurations we choose to start from a known example from the literature, Timité et al. [2010]. In a first step we will perform the exact same simulation for the cases listed in Table 3.1. The reason behind this is mostly to test if the strategy to model FSI is still valid. A sketch of the geometry is shown in Figure 3.1.

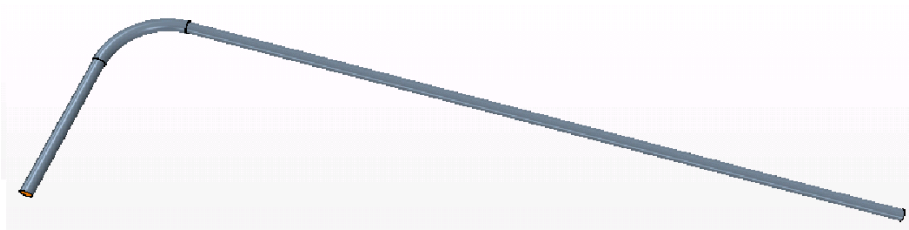

Figure 3.1: Tube Geometry

Case	1	2
Solid Properties		
Radius (R)	0.02 [mm]	0.02 [mm]
Length (L_{up})	2.5 [m]	2.5 [m]
Length (L_{out})	0.5 [m]	0.5 [m]
Radius curvature	0.22 [m]	0.22 [m]
Fluid Properties		
Reynolds number steady	600	600
Womersley number	12.14	17.17
Velocity ratio β	1	1
Density	1000 [Kg/m^3]	1000 [Kg/m^3]
Dynamic viscosity	0.001 [Pa-s]	0.001 [Pa-s]

Table 3.1: Summary of case from Timité et al. [2010]

The pulsated flow of velocity pulsation ω is then characterized by the following parameters:

- the Womersley number $\alpha = r_0(\omega/\nu)^{1/2}$, also known as the frequency parameter,

- the Reynolds number $R_e = (U * D_h)/\nu$, which for the oscillating flow we take the maximum velocity, $U_{max,osc}$, and for the steady flow we take the mean velocity $U_{m,st}$,

- the Dean number $D_n = \frac{U_m D_h}{\nu}\sqrt{\frac{D_h}{R_c}}$ where U_m is the mean velocity, ν is the kinematic viscosity, D_h is the hydraulic diameter and R_c is the mean radius of curvature.

- the ratio $\beta = U_{max,osc}/U_{m,st}$, which characterizes the balance between the steady and oscillating components of the pulsated flow,

- the oscillating velocity amplitude, defined in a flow cross-section as: $U_{osc} = U_{max,osc} * \sin(\omega t) = [\frac{1}{\pi r^2}\int_0^R 2\pi r U(r) dr]\sin(\omega t)$.

Since we are considering a fixed geometry boundary conditions, for the reasons aforementioned, our analysis will focus on the fluid behaviour. However if we are to somehow validate our model we must beforehand stipulate which parameters will serve for comparison. Since the main point of interest will be the flow profile and the secondary flow development along the bend we will compare those at the end of the bend. But before proceeding with comparing the obtained numerical results it is necessary to perform a mesh convergence. Several meshes were used and convergence of the values as well as of the residuals was obtained when reaching a 500.000.

The velocity profiles are taken along the horizontal and vertical axis of the section. Figure 3.2 and Figure 3.3 shows the results that were obtained in Timité et al. [2010] and our numerical results. As it can be seen we obtained a good fit in relation to the results from the literature. Qualitative images of the secondary flow are shown in Figure 3.4.

The evolution of the secondary flow is explained in part with the frequency parameter which can

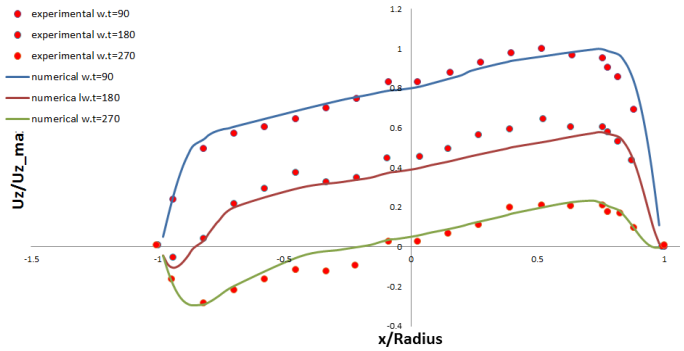

Figure 3.2: Velocity Profile x for Womersely 17.17

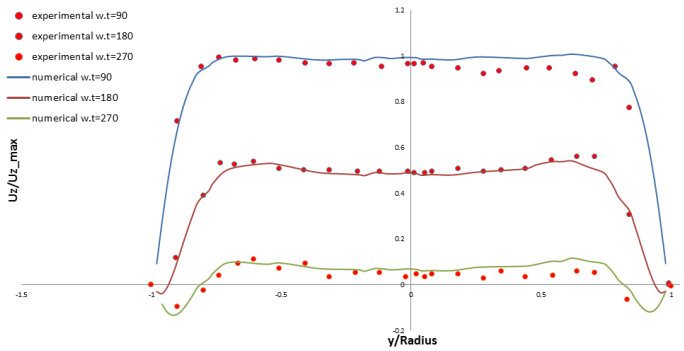

Figure 3.3: Velocity Profile y for Womersely 17.17

be defined as the ratio between the inertial forces due to the local acceleration and the viscous forces determining the movement over a time scale which is equivalent to the oscillation period. A lower Womersley number ($W_o \leq 1$) will either imply a large viscous layer near the wall, a large oscillation period compared to the viscous layer near the wall or a large oscillation period in comparison to the viscous diffusion time. When in the presence of this situation the secondary flow field will be similar to that obtained in a curved pipe with a stationary flow over the whole pulsation cycle. If however there is an increase in the Womersley number then, as expected, not only the secondary flow intensity increases but also the viscosity effect is confined to the wall region and the inertial effects increase in the central area of the section. This disequilibrium of the forces increases the effects of the centrifugal force in the cross-section centre; in the close proximity of the external wall, the tangential velocity is larger than the radial velocity and fluid particles which were close to the flow centre will start to move towards the external wall. the vortices formed at this stage will gradually stretch, and their centres will begin to move slightly to the top and bottom of the section in a symmetrical way. The axial velocity presents an annular form with a peak near the wall which coincides with the velocity at the vortex centres and a valley in the cross-section centre. The reason for the rising of the valley is due to the fluid no longer obeying the axial pressure gradient variation, in the central area, in comparison to the fluid which is close to the wall.

With even greater increase in the Womersley number the fluid close to the concave wall causes the secondary flow to stop and a stagnation zone appears close to the concave wall. The pressure gradient becomes more predominant than the centrifugal force in the section centre and in some occasions, the fluid present in the stagnation region and in the vicinity of the concave wall initiate a rotational movement.

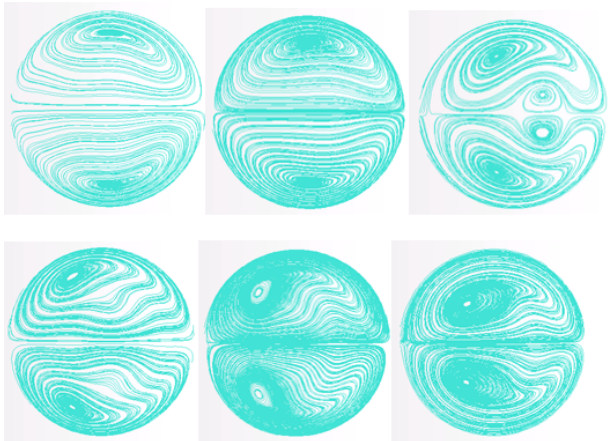

Figure 3.4: Isolines of Secondary Flow for Womersley 17.17 (upper row) and 12.14 (lower row) for the phase of 90 , 180 and 270 degree.

Near to the wall an additional pair of vortices are created and will occupy the section centre and in the same time will push the centre of the other vortices to the top and bottom of the tube cross-section. When the secondary flow presents such a configuration, with four counter rotating vortices, it is called the Lyne instability. This instability has a very complex formation process since it involves an alteration of the balance of the centrifugal force, pressure gradient and the inertial force.

One cannot however characterize the Lyne vortices by the Womersley number uniquely. As expected the Reynolds number also plays an important role. For instance, if a low Reynolds number is used then the secondary flow presents only the two Dean cells, which have a low intensity in relation to higher Reynolds numbers. In the presence of a large Reynolds number a maximum of the velocity radial distribution is found near the concave wall.

Another parameter that influences the Lyne vortices is the amplitude ratio defined as β. If this value is under the unity then a quasi-stationary flow appears. This is due to the dominance of the stationary component on the oscillating component and the velocity field distribution does not depend on the Womersley number (W_o). With a velocity amplitude equal to unity then the velocity field becomes more complicated and an annular region begins to appear. The secondary flow thus can present some particularly interesting fields depending on the Womersley number.

During the deceleration phase of a pulsated flow, if the stationary component is not too large in comparison to the time-dependent component, the fluid movement near the wall presents a reversed flow in relation to the flow in the centre of the section centre. This reverse flow increases near the convex wall. Close to the wall one can observe that the shear stress varies not only in magnitude but also in direction.

With this simulation we managed to replicate successfully the results that were obtained in Timité et al. [2010]. This is an important step since we can know proceed with the FSI experiment and see what differences will the effect of elasticity have on the fluid.

3.1.2 Flow through a $90°$ Elastic Curved Pipe

Now that the rigid case was validated we can finally study the effects of FSI. In order to save in computational time it is important to note that only upon the bend there will be an elastic tube applied. As we have seen in the other cases there might be some interference due to the fact that we fixed the extremities of the elastic tube. Even so since we do not have a laboratorial experiment in order to validate the solid deformation we will thus assume that what we have learned previously, which has proven to be quite reliable, still applies and thus the error committed is well within admissible values. Also the Rayleigh damping methodology can prove to become less accurate since we are dealing with bends and the methodology was developed with straight tubes. However this is not a reason for concern since Rayleigh damping is used in order to attenuate excessive oscillations and in this case we should not obtain those considering the low Reynolds number flow. Also we choose to use two Young modulus, the first one greater than the second, since we would like to try to establish where the rigid behaviour hypothesis would be suitable to assume. Table 3.2 presents the properties of the solid used.

Case	
Solid Properties	
Thickness	2.32 [mm]
Density	2702 [Kg/m^3]
Young Modulus 1	3 [MPa]
Young Modulus 2	0.0625 [MPa]
Poisson Coefficient	0.3
Rayleigh Damping	
Mass damping coefficient (Young Modulus 1)	-0.33996 [Hz]
Stiffness damping coefficient (Young Modulus 1)	0.004018 [s]
Mass damping coefficient (Young Modulus 2)	-0.04907 [Hz]
Stiffness damping coefficient (Young Modulus 2)	0.002784 [s]

Table 3.2: Summary of Solid Parameters

Table 3.3 presents the maximum wall displacement in relation to tube thickness obtained in the elastic pipe.

Table 3.3: Maximum Displacement in relation to tube thickness

	Young Modulus 1	**Young Modulus 2**
Thickness Displacement $Wo = 12.14$	0.05 [%]	2.32 [%]
Thickness Displacement $Wo = 17.17$	0.08 [%]	4.22 [%]

As we can see in Figure 3.3 the deformation could be considered as derisory and the use of FSI in such case would only be a waste of resources. In Figure 3.5 we present the results obtained for the velocity profiles with its respective Young modulus. As we can see, for the lower Womersley number case the velocity profile obtained with the elastic pipe shows very small deviations to the one obtained with the rigid pipe. Only in the $270°$ phase there is some difference. This is somewhat to be expected since the wall displacement is very low. However with the second case the velocity profile exhibits large differences when the lower Young modulus is applied. The margin of difference goes as high as 25%. It is essential to always keep in mind that the flow pressure in the bend region is extremely low, with a maximum of 17 Pascals. With these profiles it is very clear that flow behaviour is intrinsically

connected with the geometry deformation and vice versa. The elastic wall influences the flow through the deformation that contributes to the pressure gradient to become even more predominant than in the rigid case, which explains the reason for the differences observed.

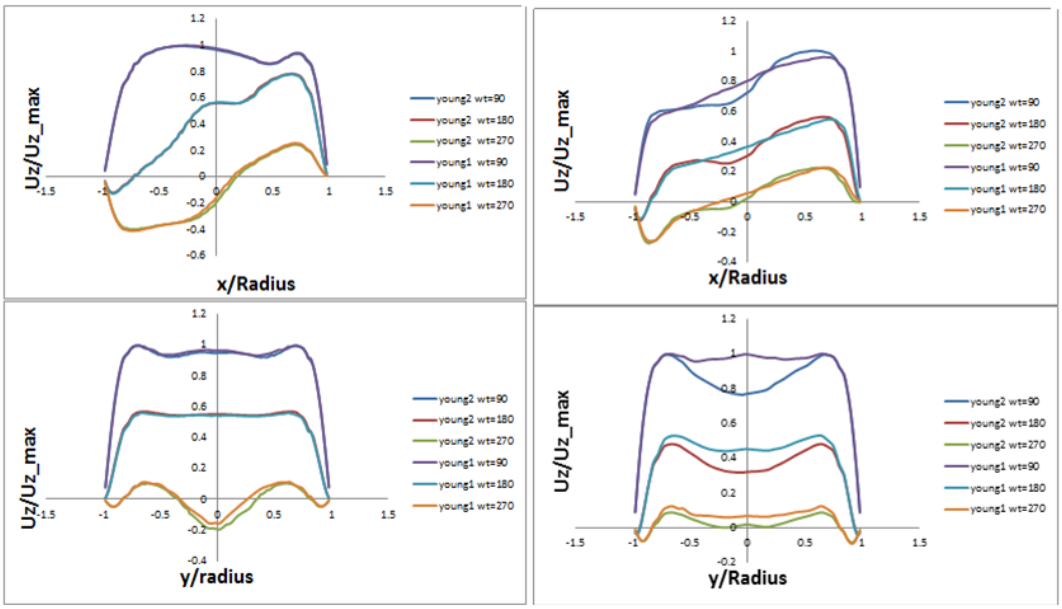

Figure 3.5: Velocity profiles left column Womersley 12.14, right column Womersley 17.17.

In Figure 3.6 we can see that the instabilities present in the flow are much more pronounced. Starting with the lower Womersley number and comparing Figure 3.4 with Figure 3.6 we see that there is a more pronounced separation between the iso-lines. This is due to the intensity of the secondary flow being greater and since we used the same scale as for the rigid case we have this spacing in the middle section. When looking for the higher Womersley value and for the the first young modulus there is not much difference. This was predictable since we know that the secondary flow is directly related to the velocity profile since it arises from the vorticity of the fluid. However when looking for the second young modulus the differences observed are quit interesting. Luckily the value of young modulus and flow regime seem to be correctly aligned in order to allow us to observe the transition of Dean flow into Lyne flow. In the 180^0 phase we see the formation of two pairs of counter rotating vortices. If we were to follow a film of the simulation we would be able to see these pairs of vortices moving along the central axis to the right side of the wall, growing further into the Lyne vortices that are seen in the 270^0. Although the literature used for this case does not refer what happens with the behaviour of wall shear stress, we decided to plot it in order to see if major differences where observed. These results are presented in Figure 3.7 and 3.8.

In Figure 3.7 there is no significant observable differences in terms of wall shear stress which was foreseeable due to what we observed before with the velocity profiles. The same does not happen when we look in Figure 3.8 we see that there is significant changes at both extremes of the horizontal axis (corresponding to 0 and 180 degrees). The zero value seen at zero radians comes from the rise in intensity in the vortices that, since they are counter rotating, cancel any tangential speed value leading to the zero wall shear stress. Now in the opposite side of the wall we see the typical signature of the

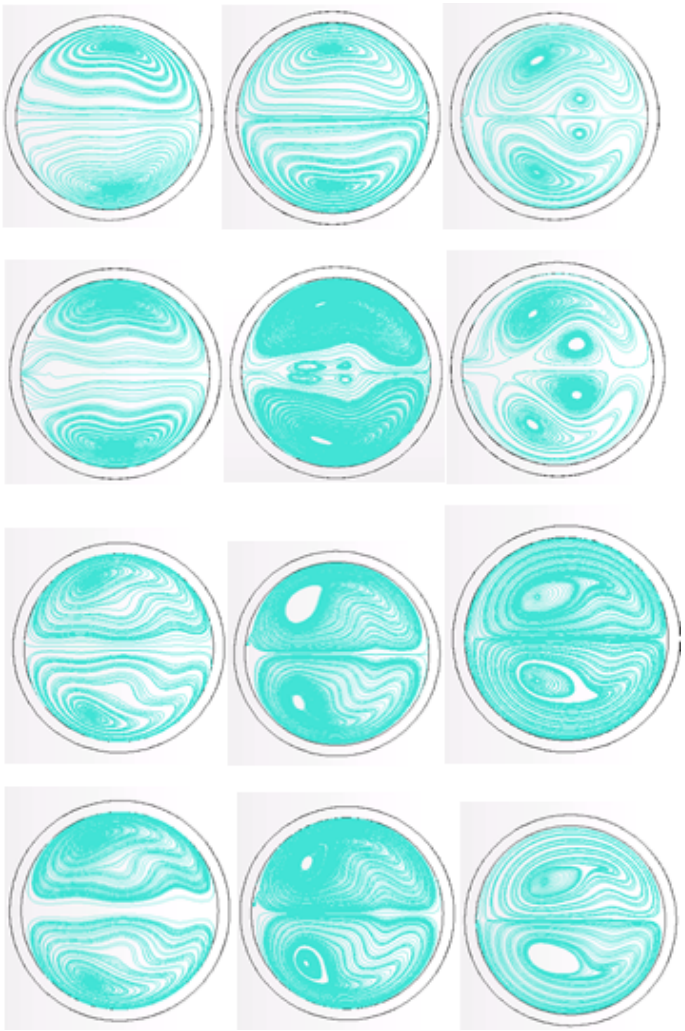

Figure 3.6: Secondary flow for Young Modulus 1 and 2, the first two rows are for Womersley=17.17 and the other two rows for Womersley=12.14.

Lyne vortices represented here as a slight depression on the maximum value.

With this simulation many important conclusions on FSI effects can be deduced. Although one may argue that the change on the wall displacement is not enough to truly justify the use of a fully three dimensional analysis, the differences observed requires that, for a certain application, some thought must be given in what we want to simulate and its final application. Since with a mere 4.22% maximum displacement in relation to wall thickness we managed to obtain differences in fluid flow profile up to 25%. For example if this tube where to be a fuel line to a combustion engine, this could be the difference between having a higher economy in the combustible spent. Another example could be made with a compressor or a turbine. If the flow has strong secondary flow instabilities this also means that the losses will be higher and the power obtained from the work would be significantly lower.

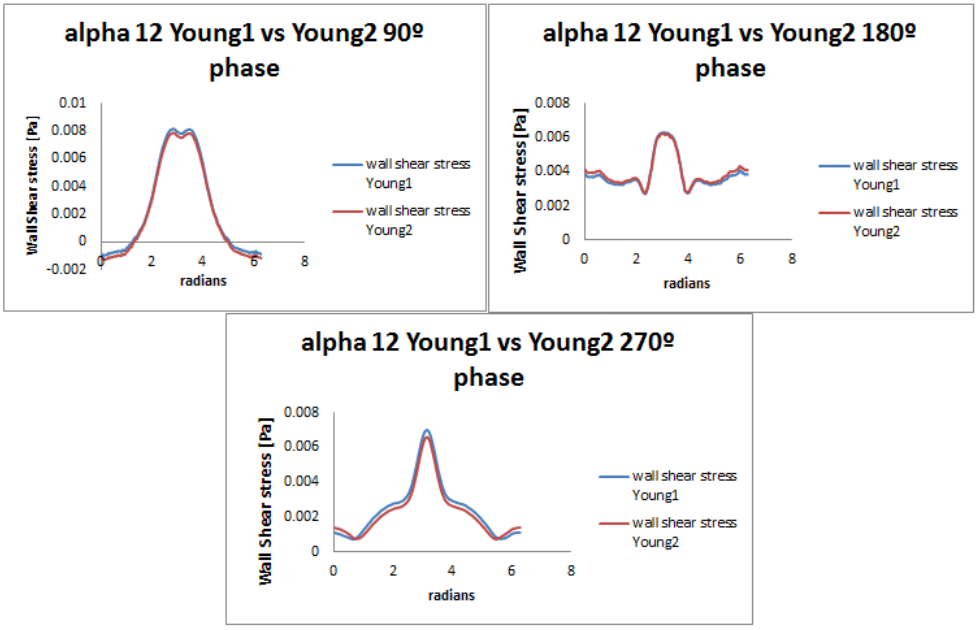

Figure 3.7: Wall Shear Stress for Womersley=12.14.

3.2 Blood Flow through an Idealized Tapered Aorta Artery

3.2.1 Introduction

We will present then the last case in our study of FSI corresponding to the blood flow simulation in an idealized aorta artery. As easy as it seems there has been already many projects and studies done upon this subject. Plus we had no access to accurate CAD geometries that could be obtained with magnetic resonance imagery, MRI. Thus we turned our research into what had been done with simplified geometries and there seemed to be one aspect which no conclusive study had already been done. It is common knowledge that as the aorta travels down the human body it starts to taper and divide itself into smaller blood vases. The study we present here seeks to answer to the question that is what happens when the wall Young modulus changes to both the aorta and the blood flow. This aspect seemed to have been overlooked since the MRI is becoming more and more accessible.

The geometry and constitution of the aorta can be quite complex. For instance the artery wall of the aorta is divided in three layers, the tunica interna or intima, tunica media and tunica externa or adventitia. Each of these have a proper constitution of fibres and muscles who can be described as a truly biological composite material. Due to understandable technical difficulties there is no accurate mechanical data to characterize each of these layers since when a person dies the muscles rapidly gain rigidity and thus only estimations have been obtained. If we add to this the fact that there is almost not even two people with the same constitution, then this task is truly gargantuan. During the literature survey the disparities that have been shown even for a single layer model can be quite astounding. For example we find young modulus varying from 1.2 MPa to 0.4 MPa. Thankfully the blood flow is not so difficult to model and there is yet much more data on that. What we then propose is a single wall layer aorta with a taper that reach 50% at the end of our section.

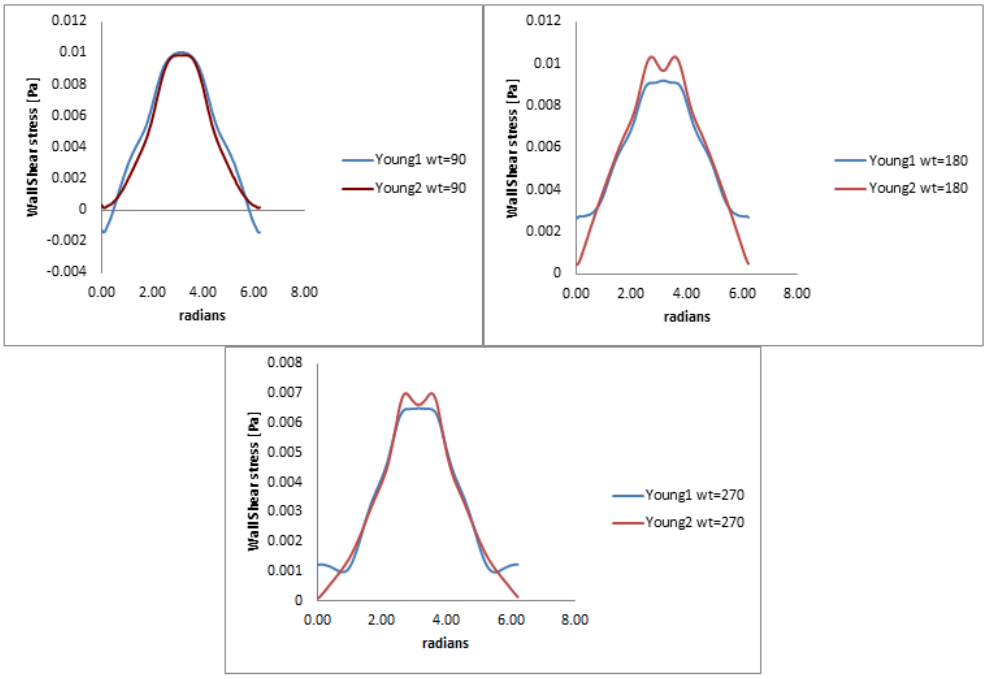

Figure 3.8: Wall Shear Stress for Womersley=17.17.

In the following table we present the characteristics of our model:

Table 3.4: Summary of aorta simulation

Case	
Solid Properties	
Radius inlet (R)	1 [cm]
Length (L)	0.351 [m]
Thickness	0.2 [cm]
Density	1000 [Kg/m^3]
Young Modulus 1-3	1.5; 1; 0.7 [MPa]
Poisson Coefficient	0.45
Fluid Properties	
density	1050 [Kg/m^3]
dynamic viscosity	0.0035 [Pa-s]

At the inlet we prescribe a mass flow rate Figure 3.9 and at the outlet an extended uniform straight tube which acts as a porous media so that an effect similar to the Windkessel model is acting on the simulation. At the end of that section a pressure condition of 6000 Pa is imposed.

As we can see these values are all within biological ranges. Since the disparities that was found when dealing with young modulus we choose to run 4 simulations. One which will be rigid and the three others will have decreasing rigidity in order to analyse the effect of elasticity. We can see in Figure 3.10 the geometry of our simplified aorta.

In this simulation the parameters which will be studied are the velocity profiles, the secondary flow, the displacement of the wall, the wall shear stress and the secondary flow structures.

The mesh used in this study has around 180000 cells and can be seen in Figure 3.11.

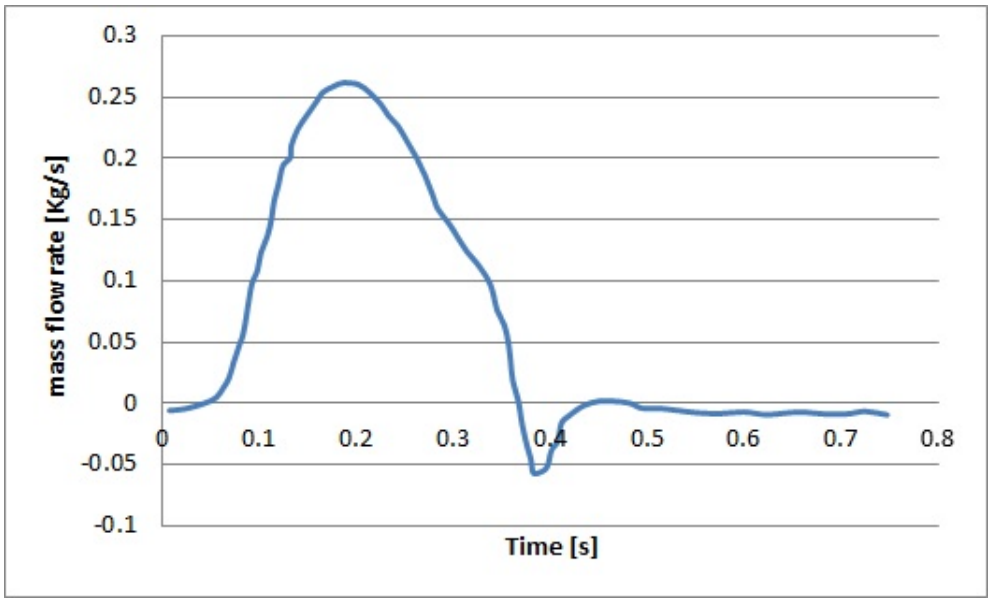

Figure 3.9: Mass flow rate at inlet of the Aorta.

3.2.1.1 Velocity Profiles

Just as we did for the third case, we will start by presenting the velocity profiles along the horizontal (z plane) and the vertical axis (y plane) of the aorta.

From the results presented in Figures 3.12,3.13,3.14, 3.15,3.17 and 3.16 we can see that the velocity profiles, taken respectively at $90°$, $180°$ and at 0.08 m in the descending section, have been affected by the elasticity of the wall considerably. At t=9.7s and t=9.88s we see that with a higher elasticity value they present a similar velocity profiles there is an increase in difference when increasing the rigidity. The peak value also changes considerably with the elasticity. For the diastole phase we have a more pronounced reversed flow with the increase in rigidity. Some of these aspects were already seen in the case of the $90°$ bend pipe. Looking at the extremes of Young modulus of 0.7 MPa and the rigid configuration we can thus conclude that:

- The velocity for each time will have a lower maximum value, in magnitude, for a more elastic configuration than for a rigid one.

- When in the diastole period (minimum flow phase), with an increase of rigidity we have a more pronounced reversed flow.

These results are physically sound since with a more elastic solid the pressure applied by the fluid on the solid walls will expand the geometry. Since the fluid has to obey the law of conservation of mass, the fluid has to lower its' speed for the same mass flow rate in a period, therefore we obtain the changes that are seen in the aforementioned profiles. It is important to keep in mind the region of the tube which as a zero velocity value observed in the case of Figures 3.13, 3.15 and 3.17 for when we will talk of the wall shear stress.

Figure 3.10: Geometry of the aorta.

3.2.1.2 Secondary Flow

Since we have curvature we already know that a secondary flow will begin to form and develop along the ascending aorta ($0°$) until the beginning of the descending aorta ($180°$). The only thing we are not sure is how the secondary flow will behave since we are also introducing taper.

As we can see in Figure 3.18 the secondary flow presents somewhat some similarities to the 90 degree bend. typical Dean vortices appear up to the $90°$, however when we go from an elastic configuration to a more rigid one we can observe that the secondary flow is capable to propagate much further into the straight tapered region (Figure 3.19). Now to be able to answer how this would happen we have to think about the physics that are behind the formation of secondary flow structures. The pair of counter rotating vortices known as the Dean vortices only appear when the pressure gradient force is centripetal and smaller than the centrifugal force in the core flow, and circumferential and greater than centrifugal force near the wall. This will result in a convective acceleration that is centrifugal in the core flow and develops a spiral pattern. With the wall exercising an increase in the centrifugal force, the difference between the extremes of the wall pressure will also increase. When the pressure gradient, that acts in-plane, becomes larger than the centrifugal force in the outer core both regions of the spiral will grow into the Dean vortices. In the core, the fluid elements are swept by the action of the centrifugal force to the outer wall. From there the flow heads towards the inner wall through a path along the lateral

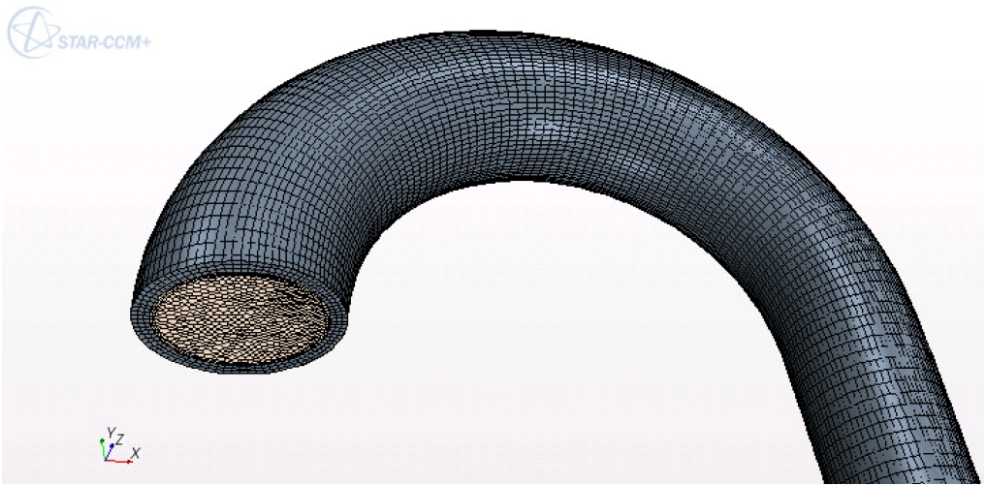

Figure 3.11: Mesh of the aorta.

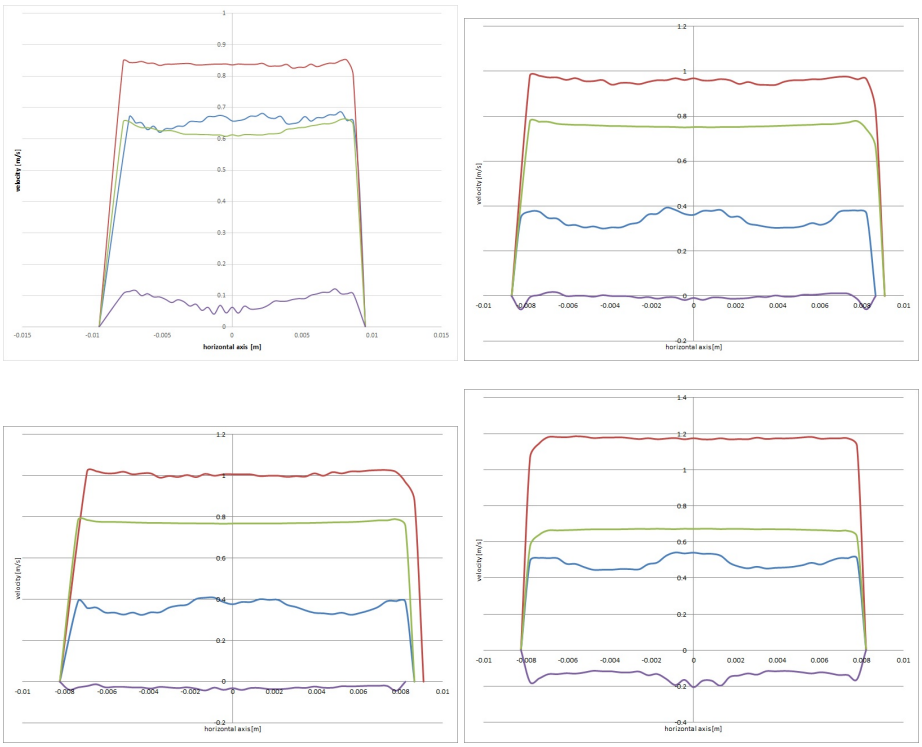

Figure 3.12: Velocity profiles along horizontal axis for section at 90 degrees for E=[0.7;1;1.5;rig] (left to right) MPa (blue - t=9.7s; red - t=9.78s; green - t=9.88s; purple - t=9,98s).

walls due to the action of the pressure gradient, the viscous forces and the centrifugal wall traction. The balance between the pressure gradient and the other two forces is what contributes for the intensity of the secondary flow. If there is an increase in the Reynolds number, then the in-plane pressure gradient, by the equilibrium law, has to also increase in order to counterbalance the centrifugal force. This will start to generate even more vorticity, which will be convected by the flow to the core where there is less viscous dissipation. This mechanism will be responsible for the beginning of the formation of other pairs of counter rotating vortices. Therefore as we can see in the pressure section, the addition of elasticity to the wall has indeed lowered even further the pressure gradient, increasing thus the pressure difference

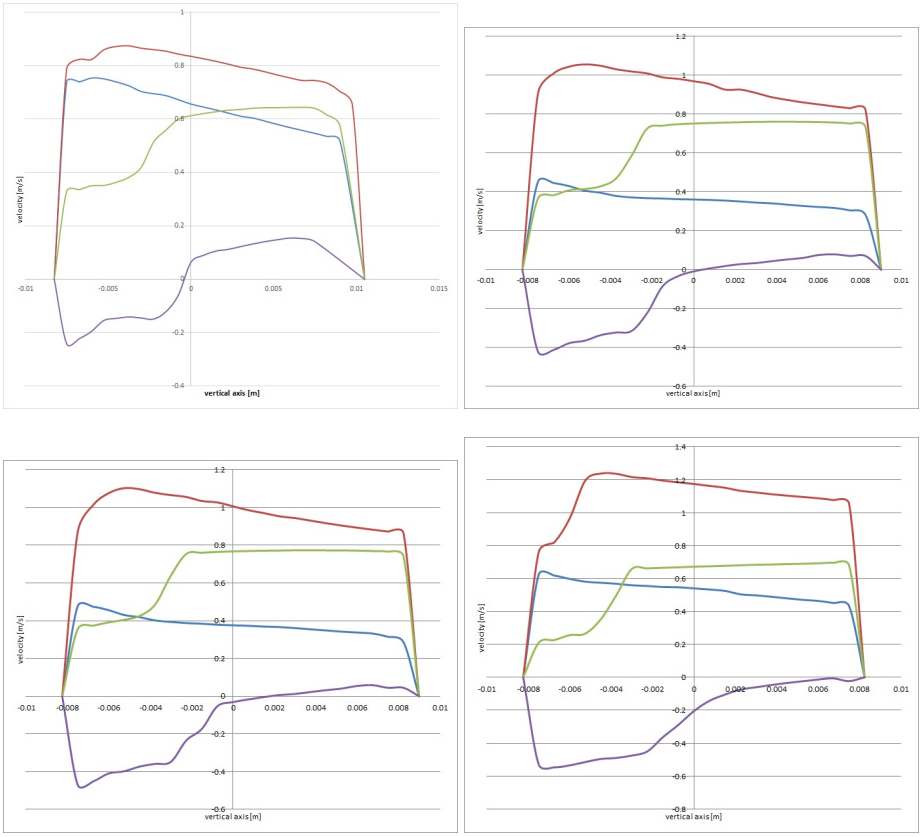

Figure 3.13: Velocity profiles along vertical axis for section at 90 degrees E=[0.7;1;1.5;rig] (left to right) MPa (blue - t=9.7s; red - t=9.78s; green - t=9.88s; purple - t=9,98s).

in-plane sections which will allow not only for the propagation of secondary flow in the straight section of the tube, but also to originate other pairs of counter vortices.

3.2.1.3 Wall Shear Stress

As we know the wall shear stress is closely connected to the velocity gradient since by its' definition it is directly proportional to the derivative of the tangential velocity. Also the wall shear stress is a very important indicator of the development of some arterial diseases. When there is a region with low wall shear stress there is the possibility of accumulation of plaques which will start to adder to the arterial wall. With time this small deposit may grow and cause a blockage, known in medical terms as a stenoses, which can very well prove fatal if critical values are reached. This is why a three dimensional analysis is extremely important since there is no way of being absolutely sure where those areas of interest might be located.

As we can see ploting only 2D wall shear stresses, Figure 3.21 can give us only very little information when compared to the 3D scenes obtained in Figure 3.22. In the two dimensional case we can extract some very interesting conclusions of what happens in the near wall region. When looking at the first and the second graph in the outer and inner wall shear stress, we can observe a similar behaviour along the entire tube with only slight variations in magnitude. The main reason being that they their respective velocity profiles (previously presented in Figures 3.12,3.13,3.14, 3.15,3.17 and 3.16) do not

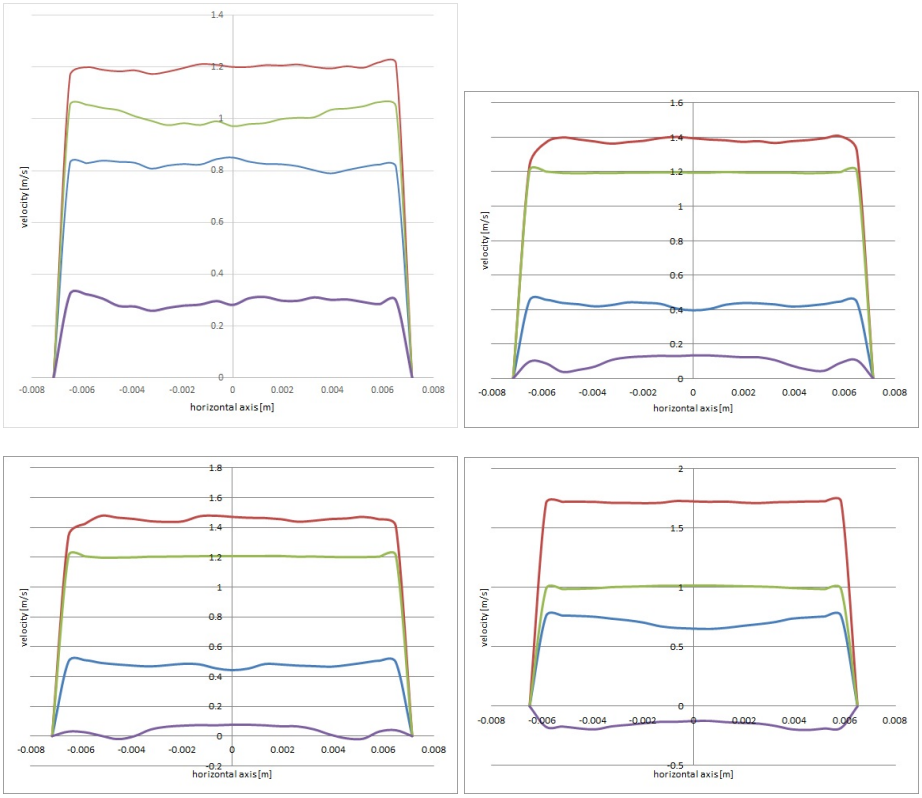

Figure 3.14: Velocity profiles along horizontal axis for section at 180 degrees E=[0.7;1;1.5;rig](left to right) MPa (blue - t=9.7s; red - t=9.78s; green - t=9.88s; purple - t=9,98s).

diverge much with the variation in the Young modulus. Now when looking at the second and the third graph we have some important differences that are of crucial importance. In the peak value we see the same tendency for the wall shear stress, but there is a significant drop on the magnitude. This is another result that prove not only that our model is working accordingly, since we have a decay up to 30% in the peak velocity value, but also proves what is seen in the literature. For a long time many doctors and engineers remained puzzled by the fact that the two and three dimensional analysis with rigid walls tended to overshoot the magnitude of the wall shear stress. We can thus see that the key for this problem came all along from the non inclusion of the fluid structure interaction of the walls into the simulation. This result thus proves that fluid structure interaction is an essential part for the study of not only hemodynamics but also any other application where a similar situation might arise. For the last graph which corresponds to the diastole phase the behaviour of the wall shear stress is more complex than the others. We must remind ourselves of what we saw in the velocity profiles, which showed the decrease of reversed flow with the increase of elasticity. That is the key in understanding the observed curves. Indeed for the curved section we can see that, in magnitude, the flow velocity is higher when in the tube is more elastic. This results in a higher derivative of velocity near the wall which will increase proportionally the wall shear stress. Now for the remaining section the boundary layer present in the straight tube is considerably lower, as we can extrapolate from the bulkier velocity profile, thus reducing the derivative which lowers the wall shear stress value.

Now when looking at Figure 3.22 we can see that the wall shear stress presents great variation

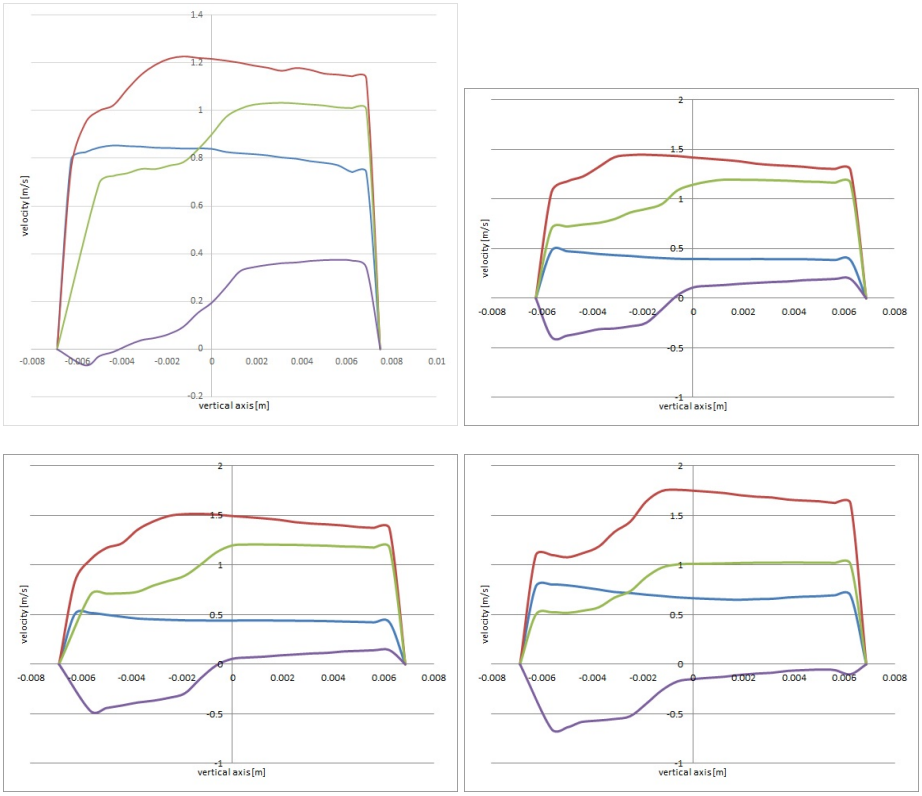

Figure 3.15: Velocity profiles along vertical axis for section at 180 degrees E=[0.7;1;1.5;rig] (left to right) MPa (blue - t=9.7s; red - t=9.78s; green - t=9.88s; purple - t=9,98s).

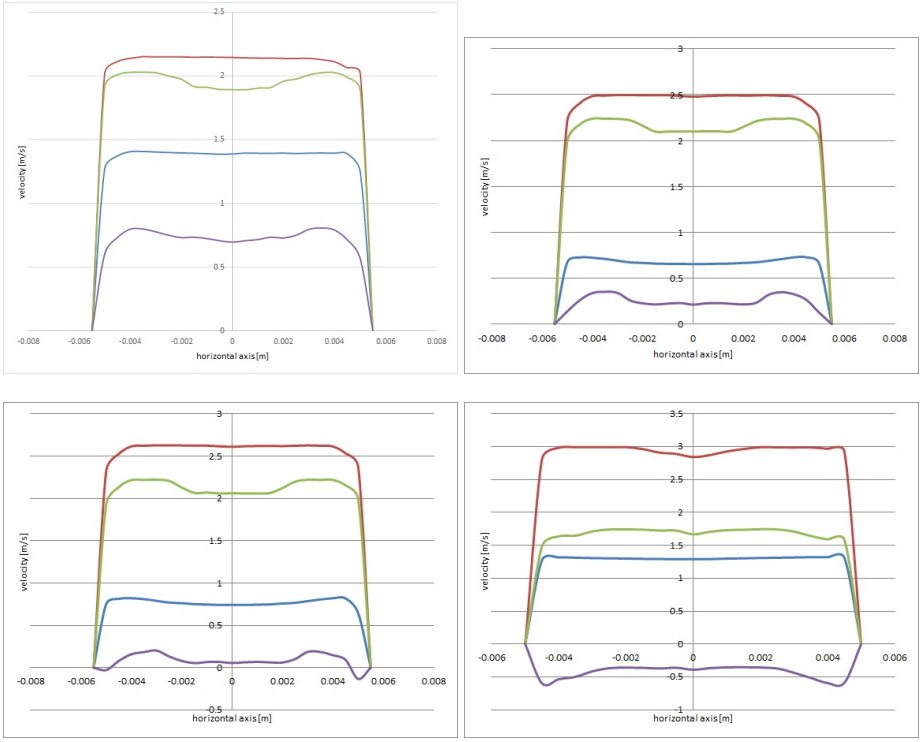

Figure 3.16: Velocity profiles along horizontal axis for section at 0.08 m in the descending section E=[0.7;1;1.5;rig] (left to right) MPa (blue - t=9.7s; red - t=9.78s; green - t=9.88s; purple - t=9,98s).

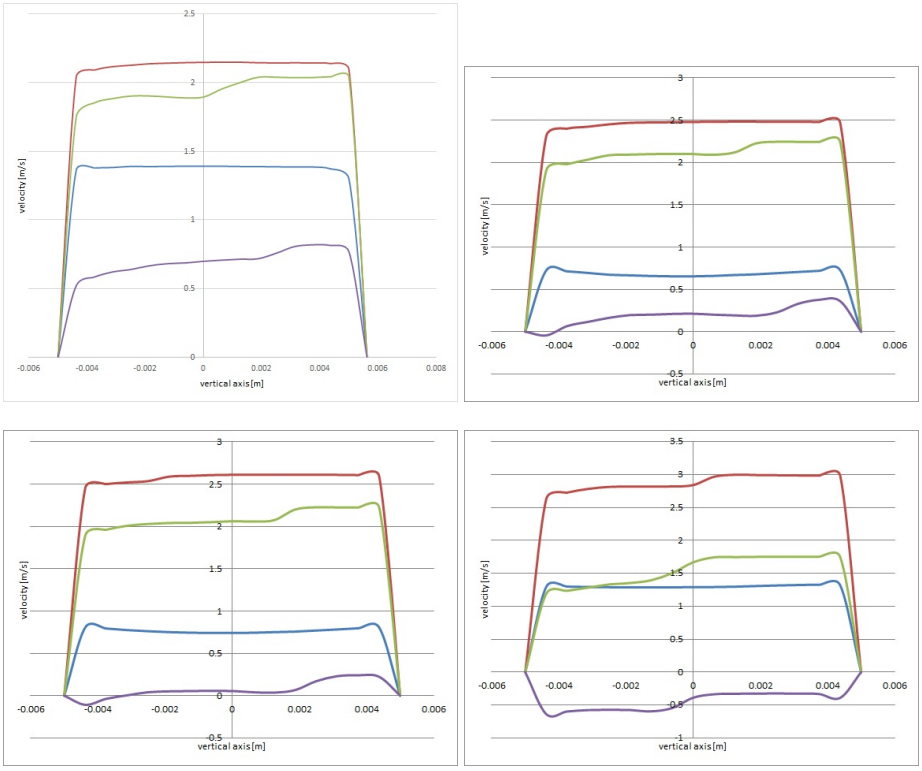

Figure 3.17: Velocity profiles along horizontal axis for section at 0.08 m in the descending section E=[0.7;1;1.5;rig] (left to right) MPa (blue - t=9.7s; red - t=9.78s; green - t=9.88s; purple - t=9,98s).

along the idealized aorta. Thus we may not affirm that with a simple two dimensional plot to be able to locate with certainty the lower values of wall shear stress. Tree dimensional plots play an important factor when trying to locate problematic areas. The most interesting feature that can be observed is the relative symmetry that appears when looking at the tube in the xy plane. This behaviour of wall shear stress is expected since we must take into account the existence of secondary flow in the tube. Also we can locate with this figures where the secondary flow starts to dissipate due to the action of viscous forces.

3.2.1.4 Pressure

As we well know it is the pressure gradient along the tube that allows the fluid to flow. But since we have a curvature we must take into account that the fluid will be not only driven by the pressure gradient, but also by the effect of the centrifugal force.

Most of what needs to be said in this section has already been related in the previous parameters. The most interesting part which has been left out and could not really be obvious when looking at velocity profiles and wall shear stress is the distribution of the pressure along the idealized aorta. In Figure 3.23 we see that there is a significant decrease in pressure magnitude, which once again comes from the fact that elasticity effects are taken into account. What was not predictable is the central distribution which for the rigid case shows a irregular form while when introducing elasticity we have a more ``rectangular ´´separation of the regions. This allows us to see how the equilibrium between the centrifugal forces,

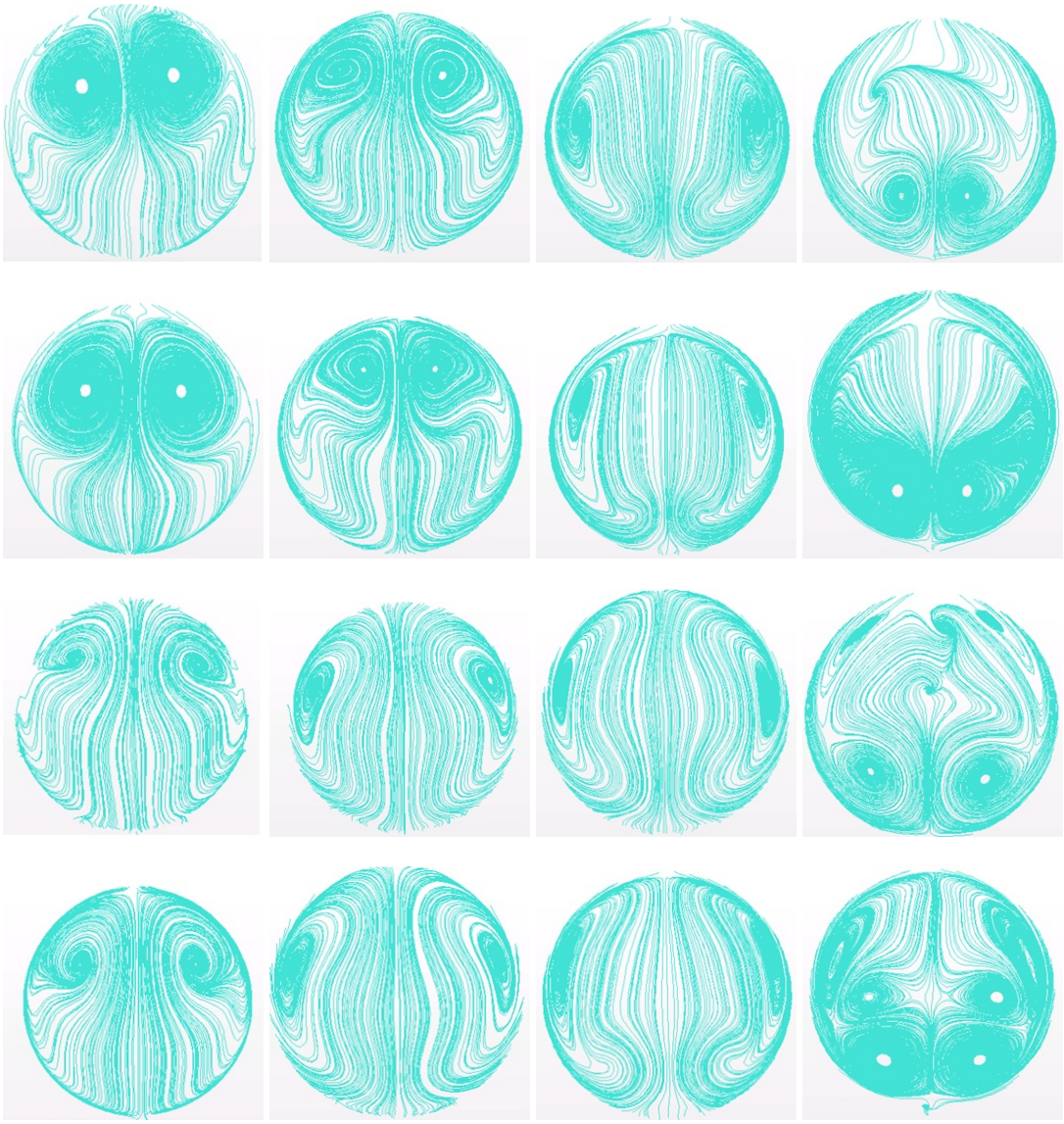

Figure 3.18: Secondary flow isolines in the midsection and exit of the curved part of the idealized aorta for E=0.7 MPa and E=1.5 MPa (columns t=9.7s; t=9.78s; t=9.88s; t=9,98s ; rows 1 and 2 section at 90 degree in the curved part and rows 3 and 4 at 180 degrees.).

viscous forces and pressure gradient interact and change with the material elasticity.

3.2.1.5 Solid Displacement

Last but not the least we present in this section the displacement of the aorta with increasing rigidity.

We can see in Figure 3.24 that the tube does not simply inflate as we could have guess. However when looking closely we can see that there is a symmetry in the xy plane. The same pattern happens when increasing the rigidity of the tube with a lower magnitude intensity, naturally. Now here the analysis is not as straightforward as we would hope for. There is a combination of several factors which have different weights in the geometry deformation. What we see is the consequence of our choices when modelling the solid. Indeed the assumption of a single layer for the arterial wall in conjunction with the isotropic material behaviour will have no doubt important consequences in the deformation obtained.

Figure 3.19: Secondary flow isolines at 0.05 m in the descending aorta for E=0.7 MPa and E=1.5 MPa (columns t=9.7s; t=9.78s; t=9.88s; t=9,98s).

Plus we have added taper, which basically acts as a strengthening of the wall. All of this as a significant impact on the entire simulation and we cannot affirm what would happen if anisotropic wall behaviour had been an option. We believe that some differences would arise but the main tendencies here observed would have remained similar.

3.2.2 Conclusion

Much was done in this simulation. Indeed not only it was possible to model the blood flow in an idealized aorta with some degree of truth but also we saw some interesting effects from the inclusion of taper which no extensive work has been found in the literature. Of course many simplifications where made and we cannot even remotely associate this to a true aortic regime. We would like to say that even so many conclusions remain useful for medical applications but also for engineering purposes.

To summarize:

- The elasticity is an important factor and that it must be taken into account in hemodynamics studies.

- Flow speed profiles will have a lower magnitude value, with the exception of the diastole regime which presents not only a slight increase in its' magnitude value but also a variation in flow direction with varying elasticity.

- The secondary flow can easily propagate into the straight section when higher elasticity values are present. Also the evolution of instability structures is different.

- the wall shear stress will present lower values with a more elastic regime, which concurs with the literature available on the subject.

Figure 3.20: Secondary flow isolines at 135 degree in the curved part ot the aorta for E=[rigid,1.5, 1, 0.7] MPa (in rows) (columns t=9.7s; t=9.78s; t=9.88s; t=9,98s).

- Pressure variation can be quite significant, around 3000 Pa, and its distribution is directly influenced by the elasticity.

- Wall deformation is not uniform cross-sectionnally and presents some circular ``spots ´´.

- Numerically speaking, there is a higher difficulty when trying to reduce the time step interval for some not well known reason. No commentaries have been found on the matter in the literature that was consulted.

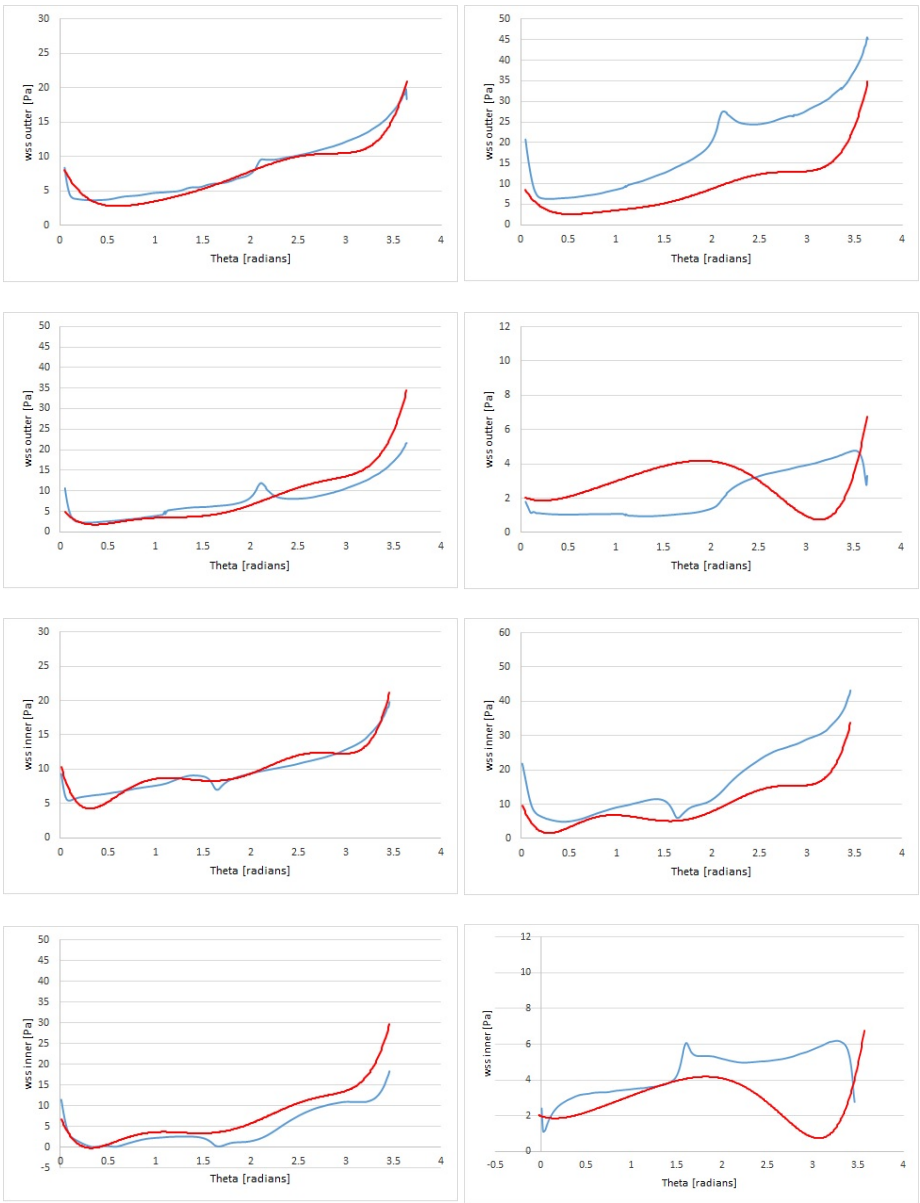

Figure 3.21: Wall shear stress along the outer (top 2 rows) and inner (lower 2 rows) wall of the tube for t=9.7s;t=9.78s; t=9.88s; t=9,98 (blue - rigid; red - E=0.7 MPa).

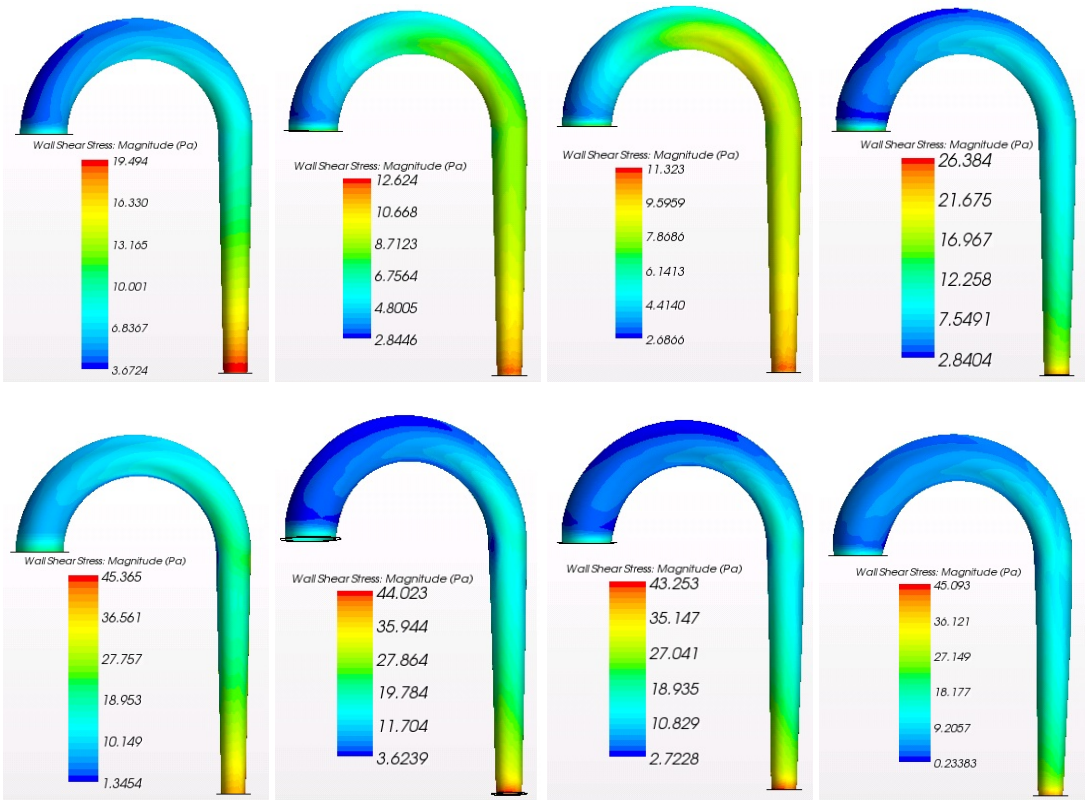

Figure 3.22: Wall shear stress on the surface of the tube and in the xy plane for E=[rigid,1.5,1,0.7] MPa at: t=9.7s (first 4 images); t=9.78s (last 4 images).

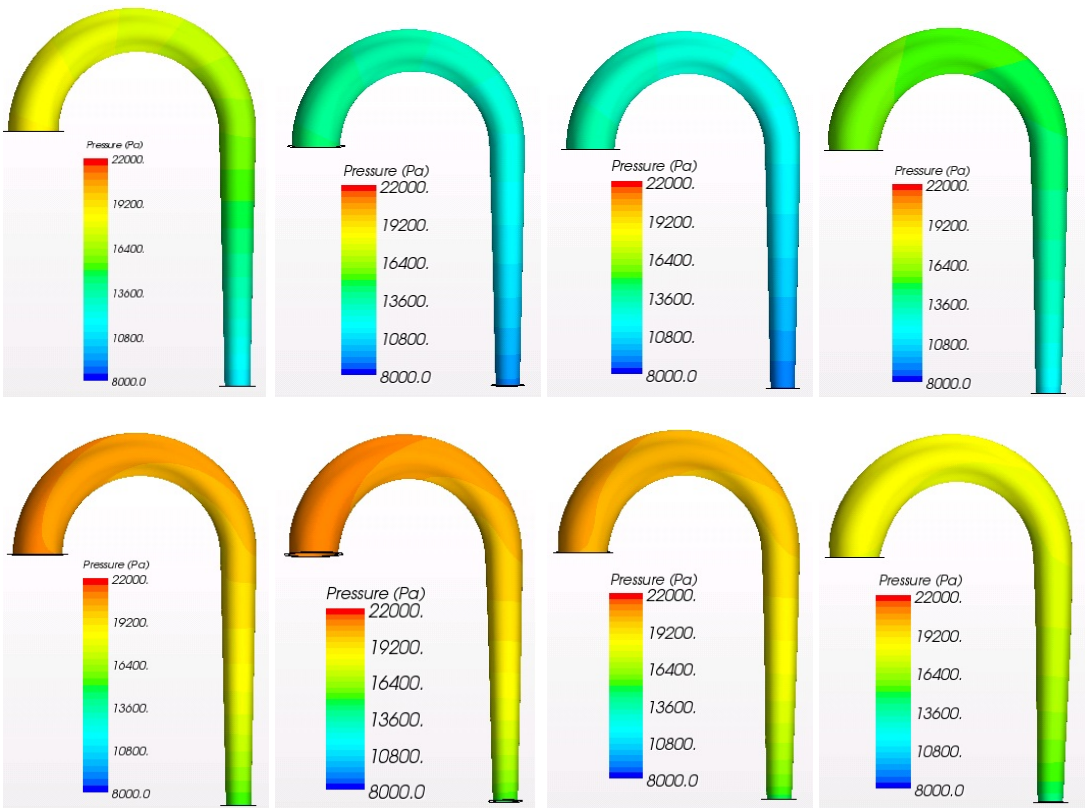

Figure 3.23: Pressure on the surface of the tube and in the xy plane for E=[rigid,1.5,1,0.7] MPa at: t=9.7s (first 4 images); t=9.78s (last 4 images).

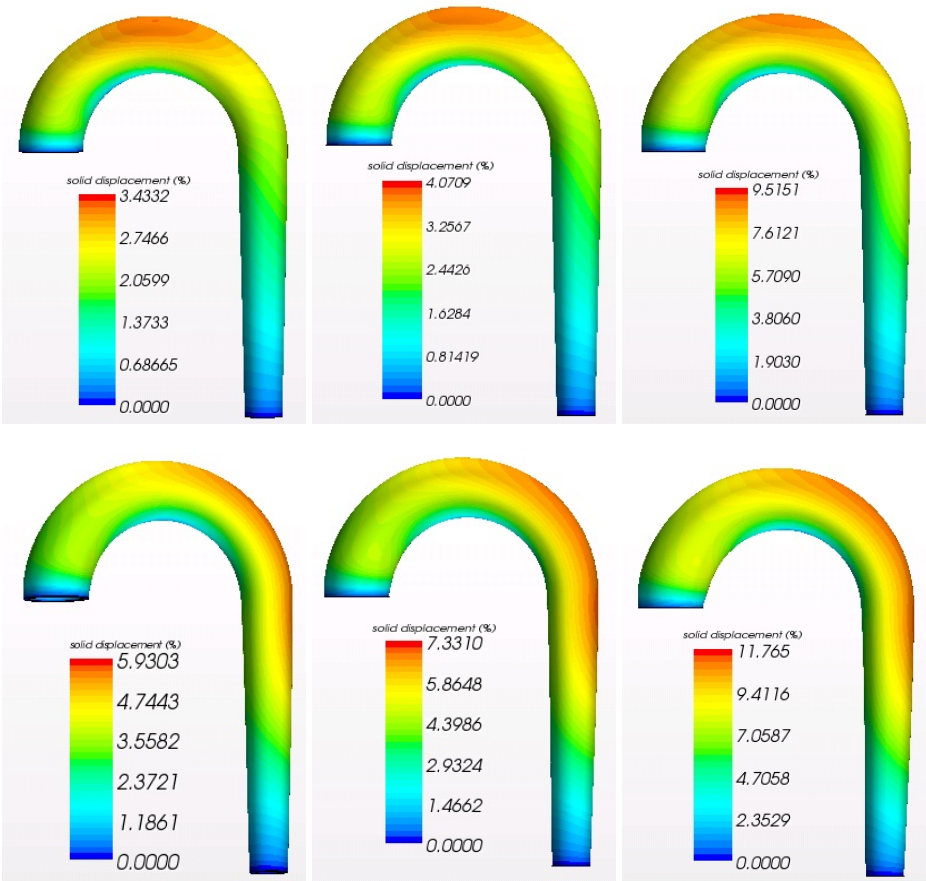

Figure 3.24: Solid displacement on the surface of the tube and in the xy plane for E=[1.5,1,0.7] MPa at: t=9.7s (first 3 images); t=9.78s (last 3 images).

Chapter 4

Conclusions

During the multiple analysis done throughout this thesis we have carefully studied and presented the relationship between elasticity and what happens in the fluid flow. Among the most important findings we conclude that:

- In the case of straight collapsible tube there is a difference between having a thinner wall and a thicker one in the sense that due to the oscillating behaviour the change in the orientation of the symmetry buckled configuration is seen as a small rotation, without any torsion.

- Pressure wave propagation is a very difficult matter to investigate since it will not only depend upon the material properties that have been chosen but also the smaller time step range required in order to capture the evolution in time frequently originates numerical blow up.

- Flow speed profiles will have a lower magnitude value, with the exception of the minimum peak which can have a variation of velocity magnitude but also may change the flow direction with varying elasticity.

- The secondary flow can easily propagate into the straight section when higher elasticity values are present. Also the evolution of instability structures is different. Dean vortices are always observed but its' evolution can result either in Lyne vortices or any other instability of the same category.

- The wall shear stress will present lower values with a more elastic regime. This has been observed as one of the most important contributions of fluid-structure interaction since it shows closer resemblance to what happens in real life.

- Pressure variation can be quite significant, around 30% and its distribution is directly influenced with the elasticity.

- Wall deformation is not uniform cross-sectionnally and presents some circular ``spots ´´.

- Numerically speaking, there is a higher difficulty when trying to reduce the time step interval for some not well known reason. No commentaries have been found on the matter in the literature that was consulted.

4.1 Achievements

With this thesis we have managed several important breakthroughs. Firstly we have successfully developed a model to simulate with the commercial software STARCCM+ fluid-structure interaction applications. This knowledge was not previously available and it had to be figured out through much trial and error. Then the results obtained showed that these simulations can be as accurate as the ones available in the literature. Thirdly it was proven that the contribution of elasticity plays a major role in the development of fluid flow through pipes. Many differences of value were noted and it is our belief that the generalization of such studies will become the norm in the near future seeing the differences that were obtained.

4.2 Future Work

Although we succeeded in implementing a numerical model to simulate day-to-day situations where FSI has an important role, there is still room for improvement. The following aspects deserve a particular attention:

- Geometry aspect: The use of an accurate representation is always crucial in a simulation, however as it was for the case of arterial flow the particularities and complexity of modelling an artery is, most of the time, daunting. For this reason it is common practice to simplify the problem by making an approximation in which some relevant conclusions might yet be made. The use of MRI technology could bring a substantial improvement to the quality and realism of the simulations. Unfortunately it was not possible to use such means in this thesis.

- Solid Mechanics: Arguably the aspect with the most potential for improvement. It is common in literature to read that what is an orthotropic material to be treated as isotropic. It is not easy to predict what differences this would bring in the results, but it is the author's belief that it should not be despised as the FSI effects where, at least not without having done some tests.

- Fluid Flow: In this part there is much work to be done due to the plethora of phenomena that are particular to some cases. One could study in more detail the evolution of the vortices and its' structure, the influence of curvature parameter, the wall shear stress variation, the influence of flow regimes,

the symmetry of secondary flow.

- Numerical code: The boundary conditions have proved in the last case to be a major challenge, either because of reflection or/and a small time step inducing volume morphing errors. The study of its' cause and ways of solving this problem would prove invaluable for improving FSI.

The work achieved in this thesis might prove to be just a step in the process of fully comprehending the immense field that is fluid-structure interaction. Nonetheless this is also part of the path of research, to try several options and then observe their differences and confront them to real results.

Bibliography

J. Alastruey, A. W. Khir, K. S. Matthys, P. Seggers, S. J. Sherwin, p. R. Verdonck, K. H. Parker, and J. Peiro. Pulse wave propagation a model human arterial network: Assesment of 1-D visco-elastic simulations in vitro measurements. *J. of Biomechanics*, 44:2250–2258, 2011.

H. B. Atabek. Wave propagation throught a viscous fluid contained in a tethered, initially stressed, orthotropic elastic tube. *Biophysical Journal*, 8:626–649, 1968.

H. B. Atabek and H. S. Lew. Wave propagation throught a viscous incompressible fluid contained in an initially stressed elastic tube. *Biophysical Journal*, 6:481–503, 1966.

H.B. Atabek and C.C. Chang. Oscillatory flow near the entry of a circular tube. *Zamp.*, 12:402–422, 1961.

M. Bathe and R. D. Kamm. A fluid-structure interaction finite element analysis of pulsatile blood flow through a compliant stenotic artery. *Journal of Biomechanical Engineering*, 121:361–369, 1999.

E. Belardinelli and S. Cavalcanti. Theoretical analysis of pressure pulse propagation in arterial vessels. *Journal of Biomechanics*, 25:1337–1349, 1992.

S. A. Berger, L. Talbot, and L. S. Yao. Flow in curved pipes. *Ann. Rev. Fluid Mech.*, pages 461–512, 1983a.

S.A. Berger, L. Talbot, and L.S. Yao. Flow in curved pipes. *Ann. Rev. Fluid Mech.*, pages 461–512, 1983b.

A.F. Bertelsen. An experimental investigation of low reynolds number secondary streaming effects associated with an oscillating viscous flow in a curved pipe. *Int. J. Fluid Mech.*, 70:519–527, 1975.

C. D. Bertram. *Eperimental studies of collapsible tubes*. Kluwer Academic Publishers, 2003.

C. D. Bertram and J. Tscherry. The onset of flow-rate limitation and flow-induced oscillations in collapsible tubes. *Journal of Fluids and Structures*, 22:1029–1045, 2006.

D. Bessems, M. Rutten, and F. van de Vosse. A wave propagation model of blood flow in large vessels using an approximate velocity profile function. *J. of Fluid Mechanics*, 580:145–168, 2007.

H. M. Blackburn and S. J. Sherwin. Formulation of a galerkin spectral element-fourier method for three-dimensional incompressible flows in cylindrical geometries. *Journal of Computational Physics*, 197: 759–778, 2004.

Z. X. Cai and X. Y. Luo. A fluid-beam model for flow in a collapsible channel. *Journal of Fluids and Strucutres*, 17:125–146, 2003.

J. Cebral, M. Castro, J. Burgess, R. Pergolizzi, M. Sheridan, and C. Putman. Characterisation of cerebral aneurysms for assessing risk of rupture by using patient-specific computational hemodynamic models. *American Journal of Neuroradiology*, 26:2550–2559, 2005.

K. C. Chang, Y. Z. Tseng, Y. J. Lin, T. S. Kuo, and H. I. Chen. Exponentially tapered t-tube model of systemic arterial system in dogs. *Med. Eng. Phys.*, 16:370–378, 1994.

L.J. Chang and J.M. Tarbell. Numerical simulation of fully developed sinusoidal and pulsatile (physiological) flow in curved tubes. *J. Fluid Mech.*, 161:175–198, 1985.

W. A. Conrad. Pressure-flow relationships in collaspible tube. *IEEE Transactions on Biomedical Engineering*, 16:284–295, 1969.

R. H. Cox. Comparison of linearized wave propagation models for arterial blood flow analysis. *Journal of Biomechanics*, 2:251–265, 1969.

W.R. Dean. Note on the motion of fluid in a curved pipe. *Philos. Mag. J. Sci.*, 4:208–223, 1927.

W.R. Dean. The streamline motion of fluid in a curved pipe. *Philos. Mag. J. Sci.*, 5:673–695, 1928.

V. Deplano and M. Siouffi. Experimental and numerical study of pulsatile flows through stenosis: wall shear stress analysis. *J. Biomech.*, 32:1081–1090, 1999.

S. Einav, S. Aharoni, and M. Manoach. Exponentially tapered transmission line model of the arterial system. *IEEE Transactions on Biomedical Engineering*, 35:333–339, 1988.

C. A. Figueroa, I. E. Vignon-Clemental, K. E.Jansen, T. J. R. Hughes, and C. A. Taylor. A coupled momentum method for modeling blood flow in three-dimensional deformable arteries. *Computer Methods in Aplied Mechanics and Engineering*, 195:5685–5706, 2006.

R. Fogliardi, R. Burrattini, and K. B. Campbell. Identification and physiological relevance of an exponentially tapered tube of canine descending aortic circulation. *Med. Eng. Phys.*, 19:201–211, 1997.

L. Formaggia, D. Lamponi, and A. Quarteroni. One-dimensional models for blood flow in arteries. *J. of Engineering Mathematics*, 47:251–276, 2003.

J. F. Gerbeau, M. Vidrascu, and P. Frey. Fluid-structure interaction in blood flows on geometries based on medical imaging. *Computers and Structures*, 83:155–165, 2005.

J. H. Gerrard. An experimental test of the theory of waves in fluid-filled deformable tubes. *Journal Fluid Mechanics*, 156:321–347, 1985.

J. B. Grotberg and O. E. Jensen. Biofluid mechanics in flexible tubes. *Annual Review of Fluid Mechanics*, 36:121–147, 2004.

C. C. Hamakiotes and S. A. Berger. Fully developed pulsatile flow in a curved pipe. *J. Fluid Mech.*, 195: 23–55, 1988a.

C.C. Hamakiotes and S.A. Berger. Fully developed pulsatile flow in a curved pipe. *J. Fluid Mech.*, 195: 23–55, 1988b.

C.C. Hamakiotes and S.A. Berger. Periodic flow through curved tubes: the effect of the frequency parameter. *J. Fluid Mech.*, 210:353–370, 1990.

A. L. Hazel and M. Heil. Steady finite-reynolds-number flows in three-dimensional collapsible tubes. *Journal of Fluids Mechanics*, 486:79–103, 2003.

A. L. Heil and O.E. Jensen. Flows in deformable tubes and channels: theoretical models and biological applications. *J. Fluid Mech.*, 195:23–55, 2003.

M. Heil. Stokes flow in collapsible tubes: computation and experiment. *Journal of Fluid Mechanics*, 353: 285–312, 1997.

F. S. Henry and M. W. Collins. A novel predictive model with compliance for arterial flow. *Advances in Bioengineering - American Society of Mechanical Engineers*, 26:131–135, 1993.

J. P. Holt. The collapse factor in the measurement of venous pressure: the flow of fluid through collapsible tubes. *American Journal of Physiology*, 134:292–299, 1941.

J. B. A. M. Horsten, A. A. van Steenhoven, and M. E. H. van Dongen. Linear propagation of pulsatile waves in viscoelastic tubes. *Journal of Biomechanics*, 22:477–484, 1989.

T. Hughes and J. Lubliner. On the one-dimensional theory of blood in large vessels. *Mathematical Biosciences*, 18:161–170, 1973.

J. Janela, A. Moura, and A. Sequeira. A 3D non newtonian fluid-structure interaction model for blood flow in arteries. *J. Comp. and Appl. Math.*, 234:2783–2791, 2010.

O. E. Jensen and M. Heil. High-frequency self-excited oscillations in a collapsible-channel flow. *Journal of Fluid Mechanics*, 481:235–268, 2003.

R. D. Kamm and T. J. Pedley. Flow in collapsible tubes: A brief review. *Journal of Biomechanical Engineering*, 111:117–179, 1989.

W. Klip. Velocity and damping of pulse wave. *Journal of Fluid Mechanics*, 1962. Martinus Nijhoff, The Hague, Netherlands.

C. S. Konig, C. Clark, and M. R. Mokhtarzaden-Dehgham. Comparison of fluid in numerical and physical models of a ventricular assist device using low and high viscosity fluids. *Journal of Biomechanical Engineering*, 116:294–301, 1999.

D. J. Korteweg. Uber die fortplanzungsgeschwindigkeit des schalles in elastischen rohren. *Annalen der Physik und Chemie*, 5:525–542, 1878.

E. Kresch and A. Noordergraaf. Cross-sectional shape of collapsible tubes. *Biophysical Journal*, 12: 1089–1098, 1972.

D. Liepsch and S. Moravec. Pulsatile flow of non-newtonian fluid in distensible models of human arteries. *Biorheology*, 21:571–586, 1984.

S. C. Ling and H. B. Atabek. A nonlinear analysis of pulsatile flow in arteries. *Journal of Fluid Mechanics*, 55:493–511, 1972.

X. Y. Luo, Z. Cai, W. G. Li, and T. J. Pedley. The cascade structure of linear instability in collapsible channel flows. *Journal of Fluid Mechanics*, 600:45–76, 2008.

W. H. Lyne. Unsteady viscous flow in rigid tube. *J. Fluid Mech.*, 45:13–31, 1971a.

W.H. Lyne. Unsteady viscous flow in a curved pipe. *J. Fluid Mech.*, 45:13–31, 1971b.

C. K. Lyon, J. B. Scott, and C. Y. Wang. Flow through collapsible tubes at low reynolds number. applicability of the waterfall model. *Circulation Research*, 47:68–73, 1980.

A. Marzo, X. Y. Luo, and C. D. Bertram. Three-dimensional collapse and steady flow in thick-walled flexible tubes. *Journal of Fluids and Structures*, 20:817–835, 2005.

Y. Meng, M. A. Rao, and A. K. Dutta. Computer simulation of the pharyngeal bolus transport of newtonian and non-newtonian fluids. *Trans. I. Chem. E. Part C: Food and Bioproducts Processing*, 83:297–305, 2005.

I. Mirsky. Wave propagation in a viscous fluid contained in an orthotropic elastic tube. *Biophysical Journal*, 7:165–186, 1968.

L. Muller and E. Toro. Well balanced high-order solver for blood flow in networks of vessels with variable properties. *Int. J. for Numerical Mehtods in Biomedical Engin.*, 2013.

J. Mynard and P. Nithiarasu. A 1D arterial blood flow model incorporating ventricular pressure, aortic valve and regional coronary flow using the locally conservative galerkin (LCG method. *Communications in Numerical Methods in Engineering*, 24:367–417, 2008.

R. M. Nerem, W. A. Seed, and N. B. Wood. An experimental study of the velocity distribution and transition to turbulence in the aorta. *Journal of Fluid Mechanics*, 52:137–160, 1971.

M. Ohmi, M. Iguchi, and T. Usui. Flow pattern and frictional losses in pulsating pipe flow. part 5: wall shear stress and flow pattern in a laminar flow. *Bull, JSME*, 24:75, 1981.

M. Olufsen, C. Peskin W. Kim, E. Pedersen, A. Nadim, and J. Larsen. Numerical simulation and experimental validations of blood flow in arteries. *Annals of Biomedical Engineering*, 28:1281–1299, 2000.

T. J. Pedley. Longitudinal tension variation in collapsible channels: a new mechanism for breakdown of steady flow. *Journal of Biomechanical Engineering*, 114:60–67, 1992.

T.J. Pedley. The fluid mechanics of large blood vessels. *Cambridge Monogr. Mech. Appl. Mathe.*, pages 160–224, 1980.

K. Perktold and G. Rappitsch. Computer simulations of local blood flow and vessel mechanics in a compliant carotid artery bifurcation model. *J. of Biomechanics*, 28:845–856, 1995.

A. Quateroni, M. Tuveri, and A. Veneziani. Computational vascular fluid dynamics: problems, models and methods. *Computing and Visualization in Science*, 2:163–197, 2000.

N.J. Rabadi, M.A. Simon, and J.C.F. Chow. Numerical solution for fully developed, laminar pulsating flow in curved tubes. *Numer. Heat Transfer*, 3:225–239, 1980.

P. Raymond, Y. Bohraus, F. Perren, F. Lazeyras, and N. Stergiopulos. Validation of a patient-specific 1-D model of the systeic arterial tree. *Am. J. of Physio. Heart and Circ. Physio.*, 301:H1173–H1182, 2010.

P. J. Reuderink, Sipkema, and N. Westerhof. Influence of geometric taper on the derivation of the true propagation coefficient using a three point method. *Journal of Biomechanics*, 21:141–153, 1988.

P. J. Reuderink, H. W. Hoogstraten, P. Sipkema, B. Hillen, and N. Westerhof. Linear and nonlinear one-dimensional models of pulse wave transmission at high womersley numbers. *Journal of Biomechanics*, 22:819–827, 1989.

A. H. Shapiro. Steady flow in collapsible tubes. *Journal of Biomechanical Engineering*, 99:126–147, 1977.

A. H. Shapiro, M. Y. Jaffrin, and S. L. Weinberg. Peristltic pumping with long wavelengths at low reynolds number. *J. of Fluid Mechanics*, 37:799–825, 1969.

S. J. Sherwin, V. Frank, J. Peiro, and K. H. Parker. One-dimensional modelling of a vascular network in space-time variables. *J. of Engineering Mathematics*, 47:217–250, 2003.

M. Siouffi, V. Deplano, and R. Pelissier. Experimental analysis of unsteady flows a stenosis. *J. Biomech.*, 31:11–19, 1998.

D. Steinman, J. Milner, C. Norley, S. Lownie, and D. Holdsworth. Image-based computational simulation of flow dynamics in a giant intracranial aneurysm. *American Journal of Neuroradiology*, 24:559–566, 2003.

D. A. Steinman and C. R. Ethier. The effect of wall distensibility on flow in a two-dimensional end-to side anastomosis. *Journal of Biomechanical Engineering*, 116:294–301, 1994.

N. Stergiopulos, D. F. Young, and T. R. Rogge. Computer simulation of arterial flow with applications to arterial and aortic stenoses. *J. of Biomechanics*, 25:1477–1488, 1992.

M. Takayoshi and N. Katsumi. Unsteady flow in circular tube (velocity distribution of pulsating flow). *Bull.JSME*, 23:186–187, 1980.

N. Takemitsu and Y. Matunobu. Numerical calculation of two-dimensional flow in the channel with a partially compliant wall. *Fluid Dynamics Research*, 4:1–14, 1988.

L. Talbot and K.O. Gong. Pulsatile entrance flow in a curved pipe. *J. Fluid Mech.*, 127:1–25, 1983.

D. Tang, C. Yang, Y. Huang, and D. N. Ku. Wall stress and strain analysis using a 3-uppercaseD thick-wall model with fluid-structure interactions for blood flow in carotid arteries with stenoses. *Computers and Structures*, 72:341–356, 1999.

C. A. Taylor, T. J. R. Hughes, and C. K. Zarins. Finite element modeling of blood flow in arteries. *Compututational Methods in Aplied Mechanics and Engineering*, 158:155–196, 1998.

B. Timité, C. Castelain, and H. Peerhossaini. Pulsatile viscous flow in a curved pipe: Effects of pulsation on the development of secondary flow. *International Journal of Heat and Fluid Flow*, 31:879–896, 2010.

T. Toshihiro, S. Kouzou, and S. Masaru. Pulsating flow in curved pipes 1:numerical and approximate analysis. *Bull. JSME 27*, 234:2706–2713, 1984.

S. Uchida. The pulsating viscous flow superposed on the steady laminar motion of incompressible fluid in a circular pipe. *Institute of Science and Technology, University of Tokyo*, 7:403–422, 1956.

A. A. van Steenhoven and M. E. H. van Dongen. Model studies of the aortic pressure rise after value closure. *Journal Fluid Mechanics*, 166:93–113, 1986.

J. von Kries. Über die beziehungen zwischen druck und geschwindigkeit, welche bei der wellebewegung in elastischen schauchen bestehen. *Festschrift der 56. Versammlung deutscher Naturforscher und Arzte gewindmet von der naturforscheden Gesellshaft zu Freiburg i. b., Supplement zu Band VIII der Berichte uber die Verhandlungen der Naturforschenden Gesellschaft zu Freiburg i. B., Akademische Verlagsbuchhndlung vor JCB Mohr (Paul Siebeck), Freibung im Breisgau und Tubingen, Germany*, pages 67–88, 1883.

J. von Kries. Studien zur pulslehre. *PhD thesis, Akademische Verlagsbuchhndlung vor JCB Mohr (Paul Siebeck)*, 1892.

R. R. Wemple and L. F. Mockros. Pressure and flow in the systemic arterial system. *Journal of Biomechanics*, 5:629–641, 1972.

N. Westerhof, F. Bosman, C. J. D. Vries, and A. Noordergraaf. Analogue studies of the human systemic arterial tree. *Journal Biomechanics*, 2:121–143, 1969.

K. Witzig. Über erzwungene wellenbegungen zaher, inkopressible flussigkeitedn in elastischen rohren. *PhD theses, University of Bern*, 1914.

J. R. Womersley. An elastic tube theory of pulse transmission and oscillatory flow in mammalian arteries. *Technical report, Wright Air Development Centre*, pages TR56–614, 1957.

J.R. Womersley. Oscillatory motion of a viscous liquid in a thin walled elastic tube i: the linear approximation for long waves. *J. Physiol.*, pages 199–221, 1954.

X. Y. Xu, Q. Long, M. W. Collins, M. Bourne, and T. M. Griffith. Reconstruction of blood flow patterns in human arteries. *Proceedings of the Institution of Mechanical Engineers Part H*, 213:411–421, 1999.

X.Zhang, R. Ajaykumar, N. M. Sudharsan, and K. Kumar. Investigation of two-dimensional channel flow with a partially compliant wall usding finite volume-finite difference approach. *International Journal for Numerical Methods in Fluids*, 49:635–655, 2005.

T. Young. Hydraulic investigations, subservient to an intended croonian lecture on the motion of blood. *Philosophical transactions of the Royal Society (London)*, 98:164–186, 1808.

R.G. Zalosh and W.G. Nelson. Pulsating flow in a curved tube. *J. Fluid. Mech.*, 59:693–705, 1973.

S. Z. Zhao, X. Y. Xu, and M. W. Collins. The numerical analysis of fluid-solid interactions for blood flow in arterial structures. part2: development of coupled fluid-solid algorithms. *Proceedings of the Institution of Mechanical Engineers Part H*, 212:241–252, 1998.

Appendix A

Appendix

A.1 Germano Referential

Germano Referential

Germano constructed a rotating coordinate system (figure 1) by considering a spatial curve described by the position vector $\hat{R}_{(\hat{s})}$ (A caret over a variable indicates that it is a dimensional quantity). The curve defines the orthonormal triad ***T***,***N***,***B***, which are respectively the tangent, normal and binormal vectors to the centreline. Germano demonstrated that, using this system, any Cartesian vector $\hat{x}$ can be expressed as:

$$\hat{x} = \hat{R}_{(\hat{s})} + \hat{r}\cos(\theta + \phi(\hat{s}) + \phi_0 N_{\hat{s}} + \hat{r}\sin(\theta + \phi(\hat{s}) + \phi_0 B_{\hat{s}}) \tag{A.1}$$

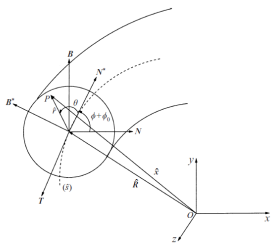

Figure A.1: Germano's coordinate system

Here $(\hat{r}, \theta)$ are polar coordinates on the cross-section. The azimuthal angle, θ, is measured from the unit vector N^* which is rotated from ***N*** by $\phi + \phi_0$, where

$$\phi(\hat{s}) = -\int \hat{\tau}(s')\,\mathrm{d}s', \tag{A.2}$$

and ϕ_0 is an arbitrary constant angle. Germano set $\phi_0 = \frac{\pi}{2}$. Using the relations

$$\boldsymbol{T} = \frac{d\hat{\mathbf{R}}}{d\hat{s}}, \quad \boldsymbol{B} = \boldsymbol{T} \times \boldsymbol{N} \tag{A.3}$$

and the Serret-Frenet formulae

$$\frac{\boldsymbol{T}}{d\hat{s}} = \hat{k}\boldsymbol{N}, \quad \frac{\boldsymbol{N}}{d\hat{s}} = \hat{\tau}\boldsymbol{B} - \hat{\tau}\boldsymbol{T}, \quad \frac{\boldsymbol{B}}{d\hat{s}} = \hat{\tau}\boldsymbol{N}, \tag{A.4}$$

Germano derived the metric

$$d\hat{x} \bullet d\hat{x} = [1 + \hat{x}\hat{r}\sin(\theta + \phi(\hat{s}))]^2 (d\hat{s})^2 + (d\hat{r})^2 + \hat{r}^2 (d\hat{\theta})^2 \tag{A.5}$$

A.2 Windkessel Model

The Windkessel Model was designed in the late 1800's by the german physiologist Otto Frank. He described the heart and the systemic arterial system as a closed hydraulic circuit. In his analogy, the circuit contained a water pump connected to a chamber, filled with water except for a pocket of air. As it's pumped, the water compresses the air, which in turn pushes the water out of the chamber. This analogy resembles the mechanics of the heart. Windkessel models are commonly used to represent the load undertaken by the heart during the cardiac cycle. It relates blood pressure and blood flow in the aorta, and characterizes the arterial compliance, peripheral resistance of the valves and the inertia of the blood flow. This is relevant in the context of, for example: the effects of vasodilator or vasoconstrictor drugs, the development of mechanical hearts and heart-lung machines.

The Windkessel model takes into consideration the following parameters while modeling the cardiac cycle:

- Arterial Compliance: refers to the elasticity and extensibility of the major artery during the cardiac cycle.

- Peripheral Resistance: refers to the flow resistance encountered by the blood as it flows through the systemic arterial system.

- Inertia: simulates the inertia of the blood as it is cycled through the heart.

The Windkessel Model is analogous to the Poiseuille's Law for a hydraulic system. It describes the flow of blood through the arteries as the flowof fluid through pipes. In this report, we focus on the electrical circuit equivalent, as shown in Figure A.2.

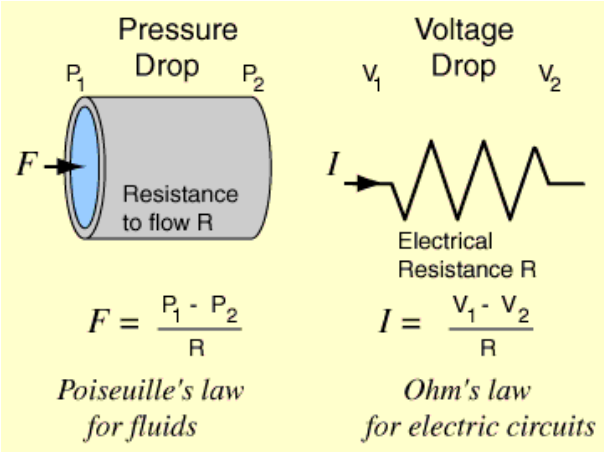

Figure A.2: Fluid Dynamics and Electrical Circuit Equivalents. Obtained from: http://hyperphysics.phy-astr.gsu.edu/hbase/electric/imgele/ohmpoi.gif

A.2.1 Model Assumptions

The following principles must be valid for the case in which a Windkessel model is to be applied:

- Cardiac cycle starts at systole.

- The period of the systole is $\frac{2}{5}th$ of the cardiac cycle.

- Arterial compliance, peripheral resistance and inertia are modeled as a capacitor, a resistor, and an inductor respectively.

The basic Windkessel model calculates the exponential pressure curve determined by the systolic and diastolic phases of the cardiac cycle. as the number of elements in the model increases, a new physiological factor is accounted for and more accurate the results arre when related to the original curve. Various other criteria such as computational complexity, shape of curve generated, etc. must be considered while deciding on which model to choose. These are approached in the three different Windkessel models explained below.

A.2.1.1 The 2-Element Windkessel Model

The simplest of the Windkessel models demonstrating the hemodynamic state is the *2-Element Model*. During a cardiac cycle, it takes into account the effect of arterial compliance and total peripheral resistance. In the electrical analogue, the arterial compliance (C in $\frac{cm^3}{mmHg}$) is represented as a capacitor with electric charge storage properties; peripheral resistance of the systemic arterial system (R in $mmHg\frac{s}{cm^3}$) is represented as an energy dissipating resistor.

the flow of blood from the heart (*I*(t) in $\frac{cm^3}{s}$) is analogous to that of current flowing in the circuit and the blood pressure in the aorta (P(t) in mmHg) is modeled as a time-varying electric potential. During

systole, as shown in Figure A.3, there is ejection of blood from the ventricles to the compliant aortic chamber. The blood stored in peripheral vessels and the elastic recoil of aorta during diastole are depicted as solid and dashed lines respectively.

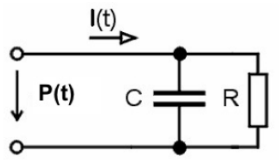

Figure A.3: Electrical Analogue of the 2-Element Windkessel Model

The theoretical modeling as seen in the electrical analogue is given as:

$$I(t) = \frac{P(t)}{R} + C\frac{dP(t)}{dt} \tag{A.6}$$

A.2.1.2 The 3-Element Windkessel Model

The 3-Element Windkessel Model simulates the characteristic impedance of the proximal aorta. A resistor is added in series to account for this resistance to blood flow due to the aortic valve. The already existing parallel combination of resistor-capacitor represent the total peripheral resistance and aortic compliance in the 2-element model as discussed before.

The theoretical modeling as seen in the electrical analogue Figure A.4 is given as:

$$(1 + \frac{r}{R})i(t) + CR_1\frac{di(t)}{dt} = \frac{P(t)}{R} + C\frac{dP(t)}{dt} \tag{A.7}$$

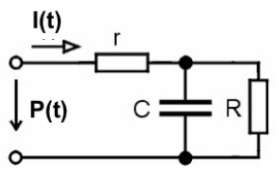

Figure A.4: Electrical Analogue of the 3-Element Windkessel Model

A.2.1.3 The 4-Element Windkessel Model

This model includes and inductor in the main branch of the circuit as it accounts for the inertia to blood flow in the hydrodynamic model. The drop in electrical potential across the inductor s given as L($\frac{di(t)}{dt}$). The 4-element model gives a more accurate representation of the blood pressure versus cardiac cycle time curve when compared to the two and the three element models. The electrical analogue is shown in Figure A.5

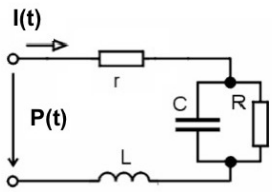

Figure A.5: Electrical Analogue of the 4-Element Windkessel Model

And its' theoretical modeling is given as:

$$(1+\frac{r}{R})i(t)+(rC+\frac{L}{R})\frac{di(t)}{dt}+LC\frac{d^2i(t)}{dt_2}=\frac{P(t)}{R}+C\frac{dP(t)}{dt} \tag{A.8}$$